Journal of Molecular Structure 1352 (2026) 144514

Contents lists available at ScienceDirect

Journal of Molecular Structure

journal homepage: www.elsevier.com/locate/molstr

Discovery of thiazolo[5′,4′:5,6]pyrido[2,3-d]pyrimidine, thiazolo[5′,4′:5,6]pyrido[2,3-d][1,3]oxazin & thiazolo[4,5-b]pyridine derivatives as novel CDK2 inhibitors: Synthesis, biological evaluation and in-silico studies

Naglaa M. Anter [a], Asmaa A. Mandour [*,b], Menna A. Ewida [b], Ahmed F. El Farargy [c], Ibrahim F. Nassar [a], Mohamed H. Sobhy [d], Abdelrahman A. Abuelkhir [e], Hoda S. El Saeed [f], Mohamed Hagras [g], Nasser S.M. Ismail [*,h]

[a] Faculty of Specific Education, Ain Shams University, Abassia, Cairo, Egypt
[b] Pharmaceutical Chemistry Department, Faculty of Pharmacy, Future University in Egypt (FUE), Cairo 11835, Egypt
[c] Department of Chemistry, Faculty of Science, Zagazig University, Zagazig, Egypt
[d] Nanomedicine Laboratories, Center for Materials Science, Zewail City of Science and Technology, 6thof October City, Giza, Egypt
[e] Analytical R&D, Hikma Pharmaceuticals, 6th of October City, Giza, Egypt
[f] Pharmaceutical Organic Chemistry, Faculty of Pharmacy (Girls), Al-Azhar University, Cairo, Egypt
[g] Department of Pharmaceutical Organic Chemistry, College of Pharmacy (Boys), Al-Azhar University, Cairo, Egypt
[h] Department of Pharmaceutical Chemistry, Faculty of Pharmacy, Ain Shams University, Organization of African Unity St., Abbassia, Cairo 11566, Egypt

ARTICLE INFO

Keywords:
Thiazolopyridine
Thiazolo-pyrido-pyrimidine
Thiazolo-pyrido-oxazin
CDK2, Cytotoxicity
Molecular modeling
Dynamic simulation

ABSTRACT:

CDK2 inhibition has emerged as a promising target and a global research area for cancer treatment that plays a crucial role in cell cycle management targeting tumor cells in a selective therapeutic approach. On account of their anticancer activities, the two privileged scaffolds benzothiazole and pyrazolo-pyrimidine were adopted in this study to design and synthesize two new series of novel small molecules featuring the hybrid thiazolo [5′,4′:5,6]pyrido[2,3-d]pyrimidine(**4–9**)&thiazolo[5′,4′:5,6]pyrido[2,3-d] [1,3]oxazin (**5,8**) in **Series 1** and the thiazolo[4,5-b] pyridine scaffolds (**3, 10–17**) in **Series 2**. Most of the synthesized compounds showed anti-proliferative activities against human cell lines lung carcinoma (A549) and breast adenocarcinoma (MCF-7). Compounds **10, 16** & **17** showed superior potency with A549 IC_{50} values of (13.50, 11.94, 12.80 μM) and (18.82, 22.77, 16.38 μM) for MCF-7, respectively when compared to Sorafenib (10.24 and 13.76 μM, respectively). The most significant enzymatic inhibitory activity was conducted by **16** and **17** against CDK2/ cyclin A2 with IC_{50} values of 13.74±0.96 and 12.09 ± 1.37 μM, respectively. Machine learning approaches including molecular docking simulation predicted a promising fitting of compounds **16** and **17** into CDK2 active site through the essential binding with Leu83 as in Roscovutine. Moreover, molecular dynamic simulations and trajectory analysis confirmed their potential inhibitory activity. Finally, ProTox toxicity model and SwissADME revealed that compounds **16** & **17** exhibited good pharmacokinetic properties aligned with the minimal cytotoxic activity results on normal cells. The essential structural features for the observed antitumor activity were also studied for the two candidates as potential selective CDK2 inhibitors.

1. Introduction

Cyclin-dependent kinases (CDK) are a group of serine/threonine kinases essential for the phosphorylation processes during cell cycle progression, transcription, and DNA repair [1,2]. They play an essential role in regulating both G1/S and G2/M cell cycle transition phase. Dysregulation or overexpression of specific CDKs disrupts normal cell cycle checkpoints, leading to uncontrolled proliferation and the development of various cancers. Among them lies CDK2 which is responsible for G1 to S-phase checkpoint regulation via phosphorylation [3–6]. Many tumor cells depend on corrupting the key component phosphorylation activity of the CDK family during cell proliferation [7,8].

The overexpression of CDKs accompanied by a decreased expression of endogenous CDK inhibitors are remarkable in various types of

* Corresponding authors.
E-mail addresses: asmaa.abdelkereim@fue.edu.eg (A.A. Mandour), nasser.mohamed@pharma.asu.edu.eg (N.S.M. Ismail).

https://doi.org/10.1016/j.molstruc.2025.144514
Received 30 August 2025; Received in revised form 14 October 2025; Accepted 23 October 2025
Available online 27 October 2025

malignancies. The cyclin dependent kinase CDK4/6 inhibitors belong to a novel drug class used for the treatment of patients with advanced breast cancer. As the activation of estrogen receptors in breast cancer, together with some other proliferation-inducing signals could stimulate the complexation of CDK4/6 with cyclin D1. Three inhibitors, palbociclib, ribociclib, and abemaciclib were approved for the treatment of HR+ and HER2- breast cancer. However, clinical applicability of these CDK4/6 inhibitors is still under investigation [9]. On the other side, CDK2 is associated with the regulatory cyclin A or E subunits that show an overexpression in human cancer including lung, ovarian, endometrial, breast, thyroid carcinomas, and others [6]. Cyclin A activation is considered an essential step for CDK2 through the progression from the S phase which showed that CDK2 is a target for most inhibitory drugs [10–11].

Heterocyclic ring systems represent powerful scaffolds with wide biological activities.[2] Also, the incorporation of several heterocyclic core in one hybrid structure, showed great interest during the design and discovery of new biologically active molecules [12–14].

Pyridine core was adopted for its known broad-spectrum bioactivities [15,16]. The pyrazolopyridine framework was considered a promising heterocyclic scaffold with reported antitumor CDK2 inhibitory activity compared to its congener-CDK2 inhibitor-Roscovitine [17–21]. Moreover, fused heterocyclic containing pyrazolopyrimidine moiety, represent common heterocycles used in the design of many pharmaceutical compounds with various medicinal applications including antitumor, anti-Alzheimer's disease, antimicrobial, anti-inflammatory, antidiabetic, and antioxidant [22–29]. In general pyridine derivatives, pyrazoloyridine, or furopyridine derivatives substituted with naphthyl and thienyl moieties exhibited antiproliferative activity [2].

Many reported replacements of purine in the lead compound Roscovitine by hybrid fused ring system including thiazolopyridine, thiazolopyrazole, thiazolopyrimidine and thiazolotriazepine proved potent CDK2 inhibitory activity [6,30–33].

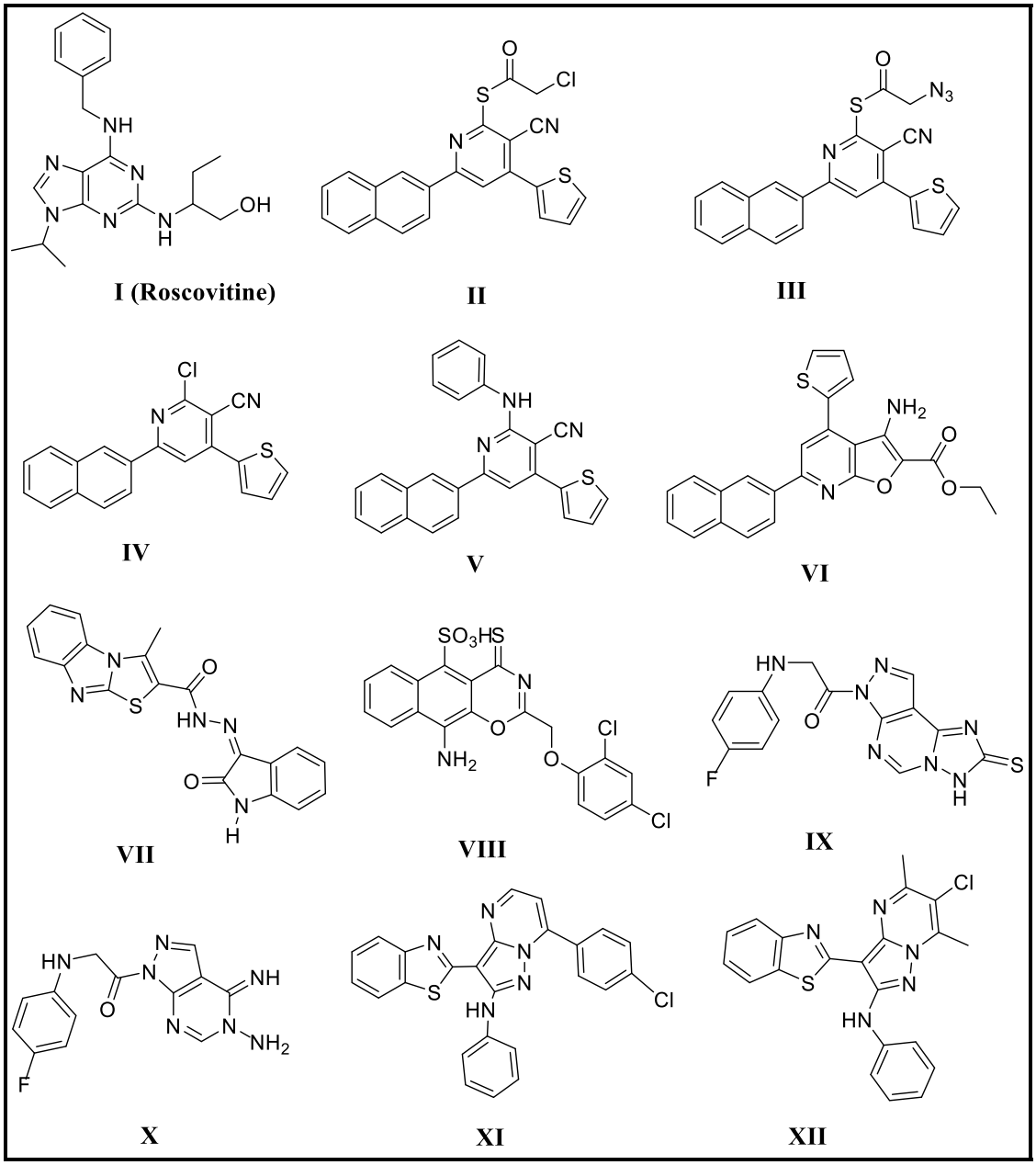

Fig. 1. Structures of previously reported CDK2 inhibitors [2,41–43].

Spiroderivatives represent a bicyclic scaffold with at least two ring entities connected through one common atom. Spirocompounds had shown importance in drug discovery targeting cancer treatment for many decades. Generally, the spirocompounds have been found with remarkable biological activities not only as anticancer but also as antimicrobial, antiviral, antioxidant, antitubercular, antileishmanial, anticonvulsant, anti-Alzheimer, hypoglycaemic, and others [34–37]. Which supports that the development and discovery of new spiromolecule-based anticancer drugs are a promising approach in medicinal chemistry field.

It is worth noting that the para-sulfonamide or meta-amino group substitution of a phenyl ring in aminothiazole hinge-binding inhibitors showed a significant potential in improving the binding interaction to CDK2. This approach could be used as guidance during the design of potent inhibitors targeting CDK2 [1,38,39].

Despite the huge advancements in cancer therapies, several limitations still persist. Including the lack of target selectivity in different cancer types, as normal cells could be affected rather than cancer cells, leading to the occurrence of numerous side effects. Also, the ability of cancer cells to produce multidrug resistance is correlated to the unresponsive outcome to conventional treatment [40]. Consequently, the discovery and development of new small molecules exerting both potency and selectivity is a challenging approach in the medicinal chemistry field.

Many efforts based on experimental and computational research studies were developed to improve the binding modes and enhance the selectivity of new CDK2 inhibitors in order to enhance potency and lower side effects. In this research the authors built a new scaffold based on a hybrid heterocyclic ring system including a spirocyclohexane ring fused with thiazolo-pyridine, thiazolo-pyrido-pyrimidine or thiazolo-pyrido-oxazin with a bio-isosteric replacement rationale compared to reported CDK2 inhibitors (Fig. 1) [2,41–43], to fulfill the needed structural features for the binding interactions within the active site of CDK2 acting as selective potent CDK2 inhibitors in two new series.

In this context, we designed and synthesized novel hybrid heterocyclic scaffolds based on thiazolo-fused pyridine, pyrido[2,3-d] pyrimidine, and pyrido[2,3-d] [1,3]oxazin cores, incorporating a spirocyclohexane moiety to improve selectivity and binding affinity toward CDK2. The design strategy relied on bioisosteric replacement of known CDK2 pharmacophores and aimed to maintain essential interactions with key active site residues, such as Leu83 and Lys89. The biological potential of the synthesized compounds was evaluated through in vitro cytotoxicity and enzymatic assays, supported by in silico docking, molecular dynamics, toxicity, and pharmacokinetic studies.

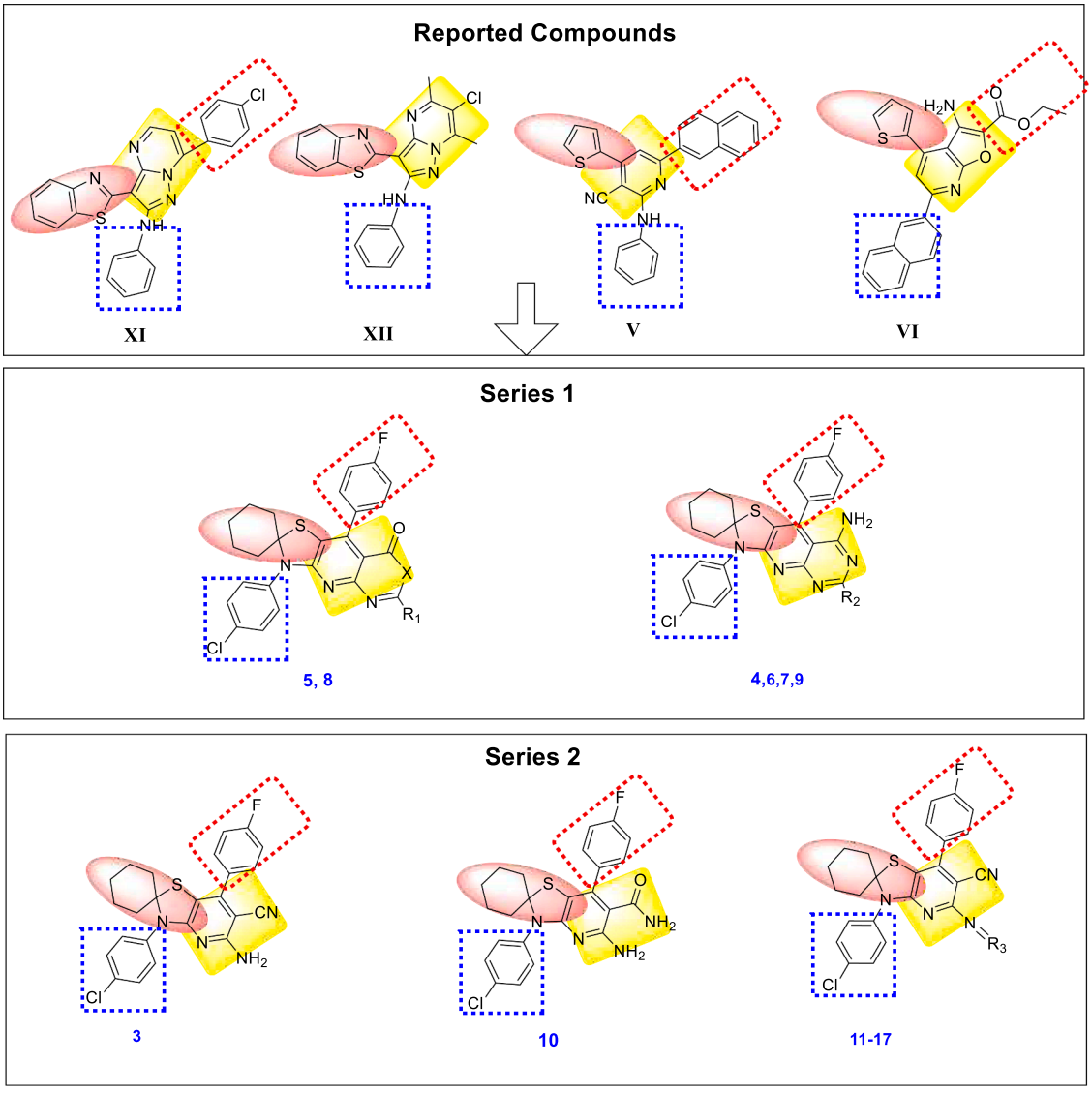

Fig. 2. Features' similarities for reported CDK2 inhibitors and the newly designed compounds.

1.1. Rational design

The design of the new compounds was based on the bioisosteric replacements of different reported ring system scaffolds in some CDK2 inhibitors (Fig. 2), by hybrid heteroaromatic spirocyclohexane scaffold constituting two series structures as follows. In **Series 1**: the heteroaromatic ring system thiazolo[5′,4′:5,6]pyrido[2,3-d]pyrimidine scaffold was applied to compounds **4,6,7&9** and thiazolo[5′,4′:5,6]pyrido [2,3-d] [1,3]oxazin was presented in compounds **5&8**. On the other side, the heteroaromatic ring system in Series 2 was: thiazolo[4,5-b] pyridin scaffold as demonstrated in compound 3 & compounds 10–17 (Fig. 2).

All the designed molecules retained the spirocyclohexane-1,2′-thiazolo scaffold by replacing the benzothiazole moiety in **XI** & **XII** and the thiophene in **V**& **VI** (Fig. 2). This hybrid ring system targeted the ATP adenine region as compared to Roscovitine maintaining the required hydrophobic bindings (Fig. 3). However, the phosphate binding region occupied by the presence of –NH linker and N7 in Roscovitine [42,44], were replaced by substitution in the fused pyridine ring to retain the binding to LEU83.

In **Series 1**, the pyrazolopyrimidine moiety in **XI** & **XII**, the pyridine in **V**, and the furopyridine in **VI** were modified to pyrido[2,3-d] pyrimidine in compounds **4,6,7&9**, and pyrido[2,3-d] [1,3]oxazin in compounds **5&8** reserving the aryl amino substituent in compounds **6,7&9** with either a 6′ keto- substitution in the pyrimidine ring in compound **6**, or 6′ thione derivative in compound **7**. While compound **3** and compounds **1017** in **Series 2** retained the pyridine ring in V (Fig. 2). The authors adopted a cyclization strategy to compounds 49 in Series 1 confirming the tricyclic ring system to mimic the binding interaction of benzimidazolthiazole in VII, naphtha-oxazin in VIII and pyrazolothiazolopyrimidine in IX (Fig. 1). The reported compounds showed a valued presence for the cyanide substituent in **II-V** and the chlorosubstituent in **II,VIII,XI** & **XII** [2,41–43]. All the synthesized compounds confirmed the p-chlorophenyl group that replaced the naphthyl moiety in **VI** and the phenyl in **V, XI** & **XII** creating **hydrophobic 1** region. And p-fluorophenyl as **hydrophobic 2** region. Also, compounds **3** & **11–17** retained the cyano substitution in pyridine ring. While compounds **4,6,7,9** & **10** showed amino substitution to the heteroaromatic ring (Fig. 2).

2. Results and discussion

2.1. Chemistry

Spirothiazolidinone derivative **2** was obtained via cyclization of Schiff's base resulted from reaction of *p*-chloroaniline and cyclohexanone with thioglycolic acid in toluene.

Spirothiazolidinone ketone **2** was treated with *p*-flourobenzaldehyde, malononitrile, and ammonium acetate to afford the key starting material **3**. A new series of heterocyclic compounds containing pyridine moieties has been obtained by allowing the 5-amino-6-cyano derivative **3** to undergo annulation reactions with different reagents. Cyclocondensation of compound **3** with formic acid yielded a pyrido pyrimidine derivative **4** which showed a new absorption band in the IR spectrum at 1672 cm^{-1} of (*C=O*) and disappearance of nitrile absorption band (Scheme 1).

Oxazinone scaffold was obtained either by allowing **3** to react with acetic anhydride to afford compound **5** or undergo benzoylation upon treatment with benzoyl chloride to afford pyrido-oxazinone derivative **8**. The reaction with benzoyl chloride took place via nucleophilic attack of the amino group on the electron deficient carbonyl group followed by releasing of a hydrogen chloride to produce a cyclized intermediate. Ultimate hydrolysis and elimination of ammonia afforded the expected pyrido-oxazinone derivative **8**. The IR spectrum of compound **8** showed a strong absorption bands at 1742 cm^{-1} (*C=O*) (Scheme 1).

Fusion of compound **3** with urea and/or thiourea at high temperature resulted in cyclization of the side chain into the pyrimidinone and pyrimidinethione derivatives (**6** and **7** respectively) which have been verified by the disappearance of the nitrile absorption bands in their IR spectra. In addition, their ^{13}C NMR of compound **6** and **7** lacked the signal for the CN group and revealed the appearance of a new signal at δ=162 and 180 ppm corresponding to the *C=O* and *C=S* respectively. Finally, condensation of **3** with the appropriate sugars and aromatic aldehydes yielded the corresponding Schiff's bases (**12–14**) and (**15–17**) respectively, which lacked the NH_2 absorption bands present in its starting material (Scheme 2).

2.2. Biological evaluation

2.2.1. In-Vitro cytotoxic activity

The cytotoxic activity of the synthesized compounds was evaluated against two human cancer cell lines: A549 (lung carcinoma) and MCF-7 (breast adenocarcinoma) [45]. The reference drug Sorafenib was used for comparison, with IC_{50} values of 10.24 μM for A549 and 13.76 μM for MCF-7. The IC_{50} was measured at a concentration of 128 μM to determine the compounds' cytotoxic potential, and the results are summarized in Table 1.

Among the tested compounds, **16, 17**, and **10** showed the most promising cytotoxic activity. Notably, compound **17** exhibited significant dual activity with potency of IC_{50} value equals to 12.80 μM (A549) and 16.38 μM (MCF-7), which was comparable to Sorafenib. Similarly, **16** showed strong cytotoxicity with 11.94 (A549) and 22.77 (MCF-7).

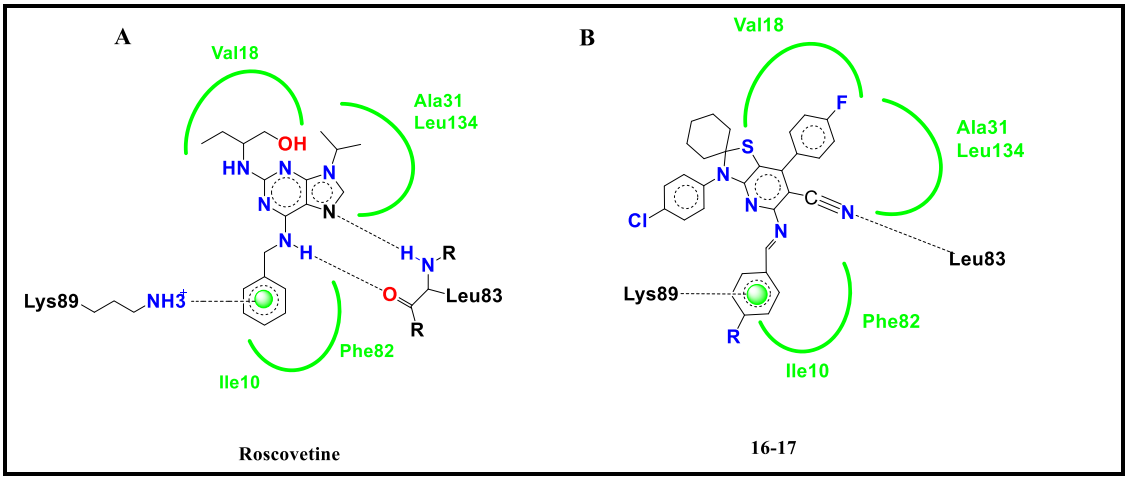

Fig. 3. The binding mode illustration at CDK2 with the key residues for **A)** Roscovitine ligand **(I)**, **B)** compounds **16 & 17** [42].

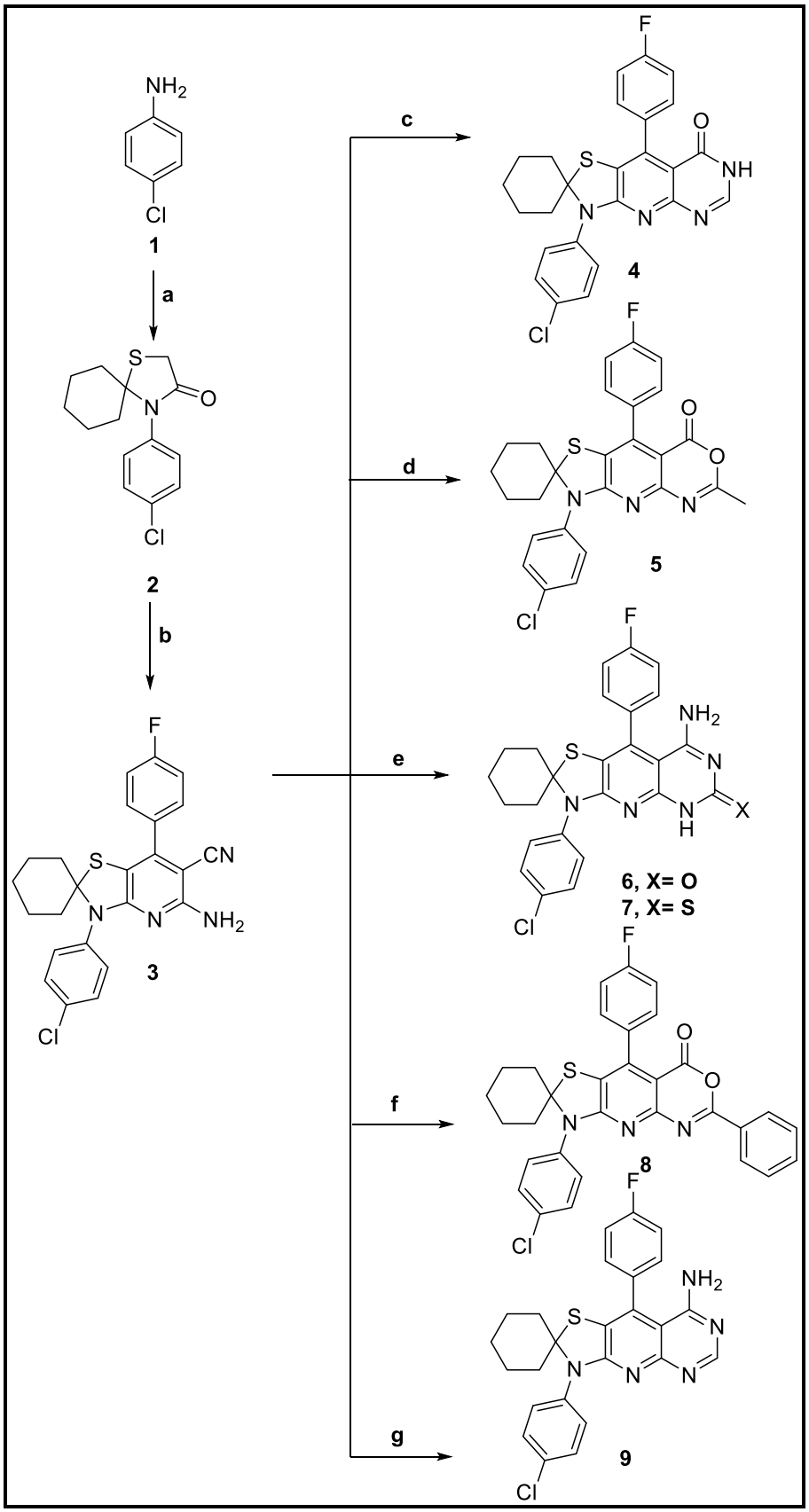

Scheme 1. Reagent and conditions: a) cyclohexanone, thioglycolic acid, toluene, reflux, 10 h. b)p-flourobenzaldehyde,malononitrile, amm. acetate, glacial acetic acid, reflux, 24 h. c) formic acid, reflux, 6 h. d) acetic anhydride, reflux, 5 h. e) urea or thiourea fusion, 280 C, 1 h. f) benzoyl chloride, pyridine, reflux, 6 h. g) formamide, reflux, 24 h.

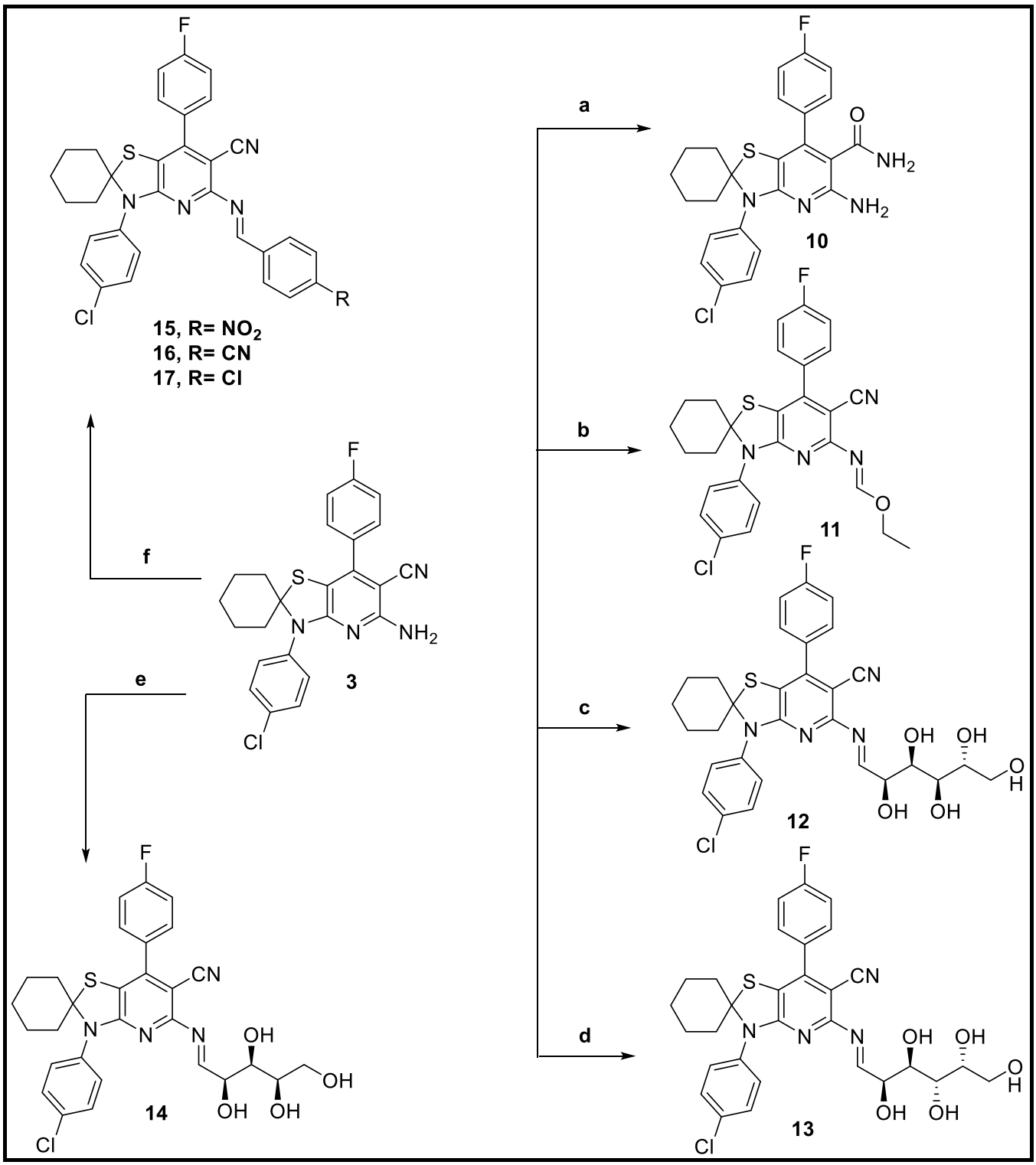

Scheme 2. Reagent and conditions: a) H_2SO_4, warming, 0.5 h. b) triethyl orthoformate, reflux, 6 h. c) D-glucose, glacial acetic acid, EtOH, 8 h. d) D-galactose, glacial acetic acid, EtOH, 9 h. e) D-xylose, glacial acetic acid, EtOH, 7 h. f) aromatic aldehyde, glacial acetic acid, EtOH, 7–8 h.

While **10** demonstrated effective cytotoxicity with IC_{50} value of 13.50 μM (A549) and 18.82 μM (MCF-7).

Compounds **8, 9** &**12** maintained good activity, particularly on A549 (21.66, 24.59 & 23.22 μM, respectively), while being also effective on MCF-7 cells. Additionally, **15** displayed moderate activity (38.45, 33.97 μM, respectively).

In contrast, compounds **4–7** & compound **11** demonstrated the lowest cytotoxic activity. These compounds may possess structural features contributing to partial inhibition.

Overall, **17, 16**, and **10** emerge as the most promising candidates for further investigation, showing cytotoxicity comparable to the standard drug Sorafenib, especially against breast and lung cancer cell lines.

Table 1
The In vitro anti-proliferative activity of the synthesized compounds against Human cell lines, Data are expressed as mean ± SD of three independent experiments ($n = 3$).

Compound ID	In vitro IC_{50} (μM) Mean ± SD	
	A549	MCF-7
Sorafenib	**10.24±3.95**	**13.76±3.48**
4	59.21±2.13	48.50±1.90
5	109.34±1.24	100.29±1.97
6	99.42±1.54	44.39±1.53
7	61.51±2.01	98.72±1.32
8	21.66±3.94	57.02±1.88
9	24.59±3.23	35.20±2.86
10	**13.50±3.42**	**18.82±3.67**
11	67.15±2.22	58.38±3.57
12	23.22±4.47	33.90±1.28
15	38.45±2.84	33.97±4.36
16	**11.94±3.51**	**22.77±2.57**
17	**12.80±2.80**	**16.38±1.67**

2.2.2. The in-vitrocyclin dependent kinase2 /Cyclin A2 enzyme inhibition:

The targeted compounds were assessed for their in vitro CDK2/Cyclin A2 enzyme inhibition assay using Promega CDK2/CyclinA2 kinase enzyme system coupled with ADP-Glo assays, the reaction was performed in four steps [46–48]. The tested compounds were assayed in the concentration of 50 μM in the presence of 5 % DMSO (Fig. 4). The percentage remaining activity was the least for the following compounds **16** & **17** with 58.32 and 57.82, respectively. Following that, the IC_{50} profiling for the promising CDK2/CyclinA2 inhibitors was tested to show the following, compound **17** with the best IC_{50} against CDK2 of 12.09 ± 1.37 μM, **16** showed IC_{50} of 13.74±0.96 μM compared to Roscovitine 0.59±0.1 μM (Fig. 5) (Table 2).

2.2.3. In vitro cytotoxicity against normal cells

The in vitro cytotoxicity of the most potent compounds **16** and **17** was evaluated against WI-38 normal cells to verify their safety and selectivity, using Staurosporine as a reference standard. Compounds **16** and **17** showed minimal cytotoxic effects on normal cells, with IC_{50} values of 45.78 and 51.16 μM, respectively compared to the reference standard IC_{50} values of 28.87 μM. These findings suggest that the newly synthesized compounds exhibit significantly lower cytotoxicity against normal cells, approximately half that observed in cancer cell lines, confirming their potential as safe therapeutic candidates.

2.3. In silico studies

2.3.1. Molecular docking

Molecular docking study was applied using C-Docker algorithm in Discovery Studio 4.0 Software. The promising compounds that showed potential CDK2 inhibitory activity (compounds **16** & **17)** were successfully prepared and docked to the active site of CDK2 enzyme. The binding modes of the designed compounds were analyzed to interpret the biological activity and to explain the interactions with the key amino acid residues in the binding site. The X-ray crystallographic structure of the target CDK2 being complexed with ligand Roscovitine downloaded from PDB as (PDB ID: 2A4L) [49,50], revealed the two hydrogen bonds with LEU83 after re-docking of Roscovitine showing validation with RMSD value equals 0.5A°. The best selected pose out of ten poses for each docked compound that mimics the binding mode of the ligand is saved as the best pose. The presented docking study showed comparable binding modes between the lead compound and the two most promising newly synthesized molecules against the essential amino acids at the active site with comparable C-Docker interaction energy (Fig. 6).

Table 3 presented the detailed docking results observed by the two docked compounds named **16** & **17** and revealed the essential binding with LEU83 via cyanide substitution on the fused pyridine ring plus the hydrophobic interaction between pyridine and ILE10 & LEU134 (Fig. 6). In addition to hydrophobic interaction between the p-fluorophenyl ring (**hydrophobic 2** region) with VAL18, ALA31, LYS33, PHE80 & ALA144. The thiazolopyridine moiety positioned the compounds in the active pocket via interaction with VAL18 (Fig. 6).

A pi-cation bond through the para substituted phenyl ring next to the imine linker with LYS89 was also observed. The preliminary predictive *in silico* study of the binding mode after docking is considered an essential tool to predict and explain the biological results [42,44]. The schematic illustration in Fig. 3 demonstrates a comparable binding mode of the two studied new compounds compared to Roscovutine ligand at the active site of CDK2 with close C-Docker interaction energy **(E)** (Fig. 6), which predicts a comparable inhibitory activity at the targeted site.

2.3.2. Dynamic simulation

The objective of performing molecular dynamic (MD) simulations and trajectory analysis was to investigate the stability of the interaction between the docked ligands and CDk2, which plays a crucial role in determining their potential as inhibitors. For this purpose, the most bioactive conformers of compounds **16** and **17** were chosen to monitor their behavior during the simulation. As depicted in Fig. 7, the total energy values remained within the range of –4378 to –4288 kcal/mol

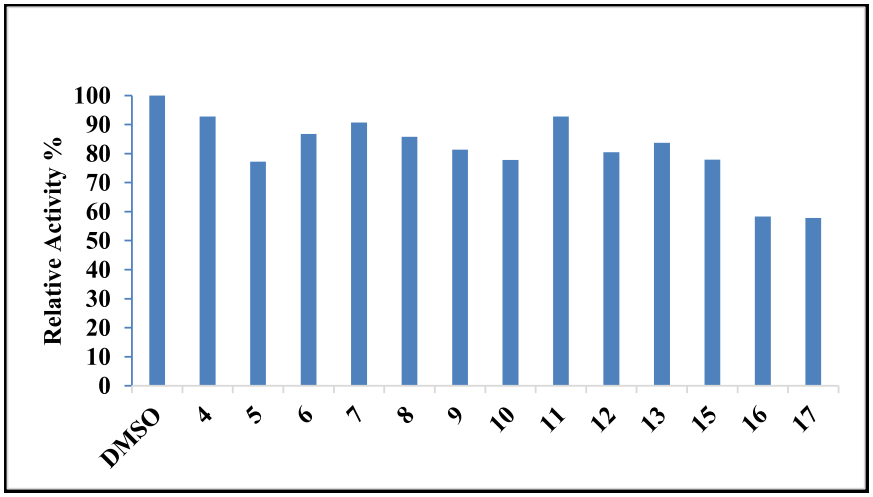

Fig. 4. Inhibition of CDK2/CyclinA2 by new compounds at 50 μM.

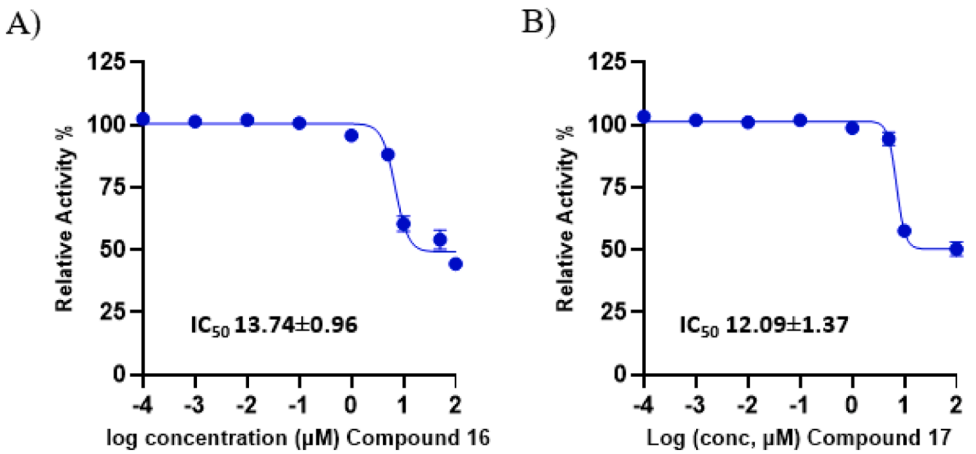

Fig. 5. The dose–response curves show the Inhibitory Concentration at 50 % (IC_{50}) curves of compound **16 A) and** compound **17 B**) in CDK2/Cyclin A2 protein kinase activity assay.

Table 2
CDK2/Cyclin A2 inhibitory activity results of the most potent compounds. Data are expressed as mean values of two independent experiments (n = 2).

Compound ID	Relative activity %
DMSO	100
4	92.82
5	77.20
6	86.73
7	90.71
8	85.78
9	81.32
10	77.83
11	92.79
12	80.43
13	83.72
15	77.89
16	**58.32**
17	**57.82**

throughout the simulation time frame (26 to 224 ps), reflecting a consistent and energetically stable interaction with the target protein [51].

To further evaluate the stability of the ligand–protein complexes, RMSD (Root Mean Square Deviation) analysis was conducted [51]. The RMSD values (Fig. 8), which varied between 0 and 1.56 Å, indicated that the structural deviation from the initial configuration was minimal, suggesting that the complexes retained their integrity over time.

Moreover, RMSF (Root Mean Square Fluctuation) was employed to examine the flexibility of individual residues within the protein during binding [51]. The observed RMSF values (0.76 to 8.29 Å) suggest limited fluctuation, pointing toward strong and rigid interactions between the ligands and CDK-2 (Fig. 9).

Altogether, the results of the simulation confirm that the complexes are dynamically stable and support the potential inhibitory effect of the compounds investigated.

2.3.3. Toxicity prediction using protox 3.0 webserver

A toxicity model was presented using ProTox 3.0 webserver to investigate the predicted toxicity of the two promising compounds **16** & **17** based on structural similarity analysis of previously known toxic fragments [52].

Compounds **16** & **17** were fed to the server through SMILES (Simplified Molecular-Input Line Entry System) using SwissADME online tool [52,53]. The two tested compounds were considered non-toxic as class 4 toxicity prediction with predicted lethal dose (LD50) equal to 800 mg/kg. Both compounds **16** & **17** showed similar Organ toxicity with high prediction probability (exceeds 0.7), as nephrotoxicity prediction probability was (0.72) and respiratory toxicity probability was predicted to be (0.78). Also, BBB-barrier prediction probability of 0.90, and Ecotoxicity (0.71) were observed. Moderate probabilities (<0.7) for clinical toxicity of (0.58) and (0.68) for Cytochrome CYP2D6 were predicted (Fig. 10).

On the other side both compounds **16** & **17** showed high inactive probability prediction (non-toxic) in the range of (0.72–0.99) towards other organ toxicity predictors including Nephrotoxicity and Cardiotoxicity, Toxicity end points immunotoxicty & cytotoxicity, all Tox21-Nuclear receptor signaling pathways, most Tox21-Stress response pathways, most Molecular Initiating Events and one Metabolism (CYP) predictor. Also, both compounds showed inactive prediction (nontoxic) with probability range (0.55–0.67) towards Hepatotoxicity, Carcinogenicity, Mutagenicity, Nutritional toxicity, Aromatase signaling, Mitochondrial Membrane Potential (MMP), a few Molecular Initiating Events and most of metabolism (Fig. 10).

The presented toxicity prediction study showed good profile for both compounds **16** & **17** over wide range of predictors compared to related compounds,

2.3.4. In silico predictive ADME study

The pharmacokinetic properties of the two tested compounds (**16** & **17**) were predicted using SwissADME online tool. [53] Results showed low GIT absorption with low BBB penetration, preferring their safe usage without CNS effect. The bioavailability radar chart presented in Fig. 11 showed the existence of the tested compounds in the desired pink region within the six parameters such as; FLEX (Flexibility), LIPO (Lipophilicity), INSOLU (Solubility), INSATU (saturation), SIZE and POLAR (Polarity) (Fig. 11). Moreover, the two compounds were predicted to be inhibitors to the Cytochrome P450 2D6.

2.3.5. Structure activity relationship

The hybrid ring fusion in thiazolo[4,5-b]pyridin scaffold presented in compounds (**16&17)** was studied to predict the essential pharmacophoric features for the biological activity. As the *in-vitro* antiproliferative activity results were co-aligned to the *in-silico* predictions showing that compounds **16** and **17** revealed the best cytotoxic activity. The hybrid heteroaromatic spirocyclohexane scaffold was believed to insert the studied compounds into the hydrophobic ATP adenine binding region. The cyanide substitution to the pyridine ring was essential to undergo the reported hydrogen bond compared to Roscovitine lead compound. Also, the two hydrophobic regions: **hydrophobic 1** and **hydrophobic 2** encouraged the correct locating to the two compounds for the best fitting results. While the phenyl ring confirmed pi-cation binding (Fig. 12).

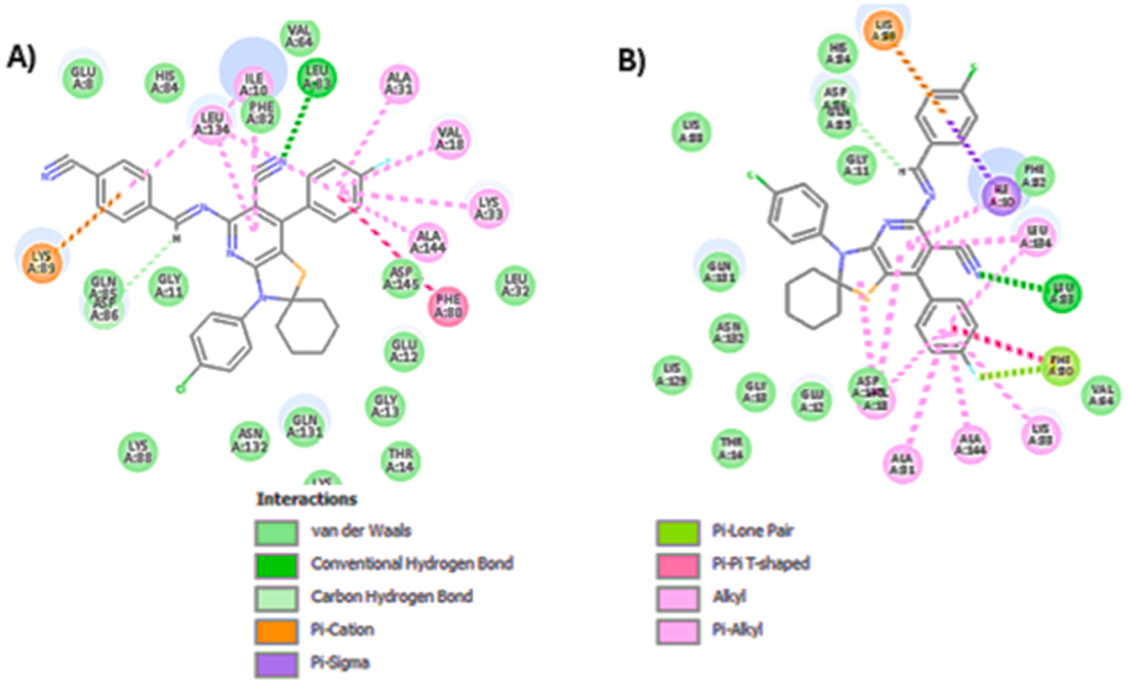

Fig. 6. The 2D-diagram showing docking results on Human cyclin-dependamt kinase 2 **CDK2 (PDB ID: 2A4L)** active sites with: **A)** compound **16** (***E*=-56.52 Kcal/mol**) and **B)** compound **17** (***E*=-52.68 Kcal/mol**).

2. Conclusion

Two new series of novel small molecules targeting CDK2 were designed and synthesized featuring a hybrid scaffold in **Series 1** of thiazolo[5′,4′:5,6]pyrido[2,3-d]pyrimidine(**4–9**) and thiazolo[5′,4′:5,6] pyrido[2,3-d] [1,3]oxazin in compounds (**5,8**). And **Series 2** compounds (**3, 10–17**) of thiazolo[4,5-b] pyridine scaffold. Most of the compounds showed cytotoxic activities against A549 and MCF -7. Compounds **10, 16** and **17** showed the most significant cytotoxic activities compared to Sorafenib. Moreover, Compounds **16** and **17** revealed the most inhibitory activity against CDK2/cyclin A2. The *in-silico* studies included molecular docking revealed comparable binding mode with the key residues compared to Roscovitine ligand. In addition to molecular dynamic simulations and analyzing trajectory studies ensured their inhibitory potential with sufficient stability. Toxicity prediction together with pharmacokinetic properties using ProTox and SwissADME were performed, and results were aligned with normal cell toxicity for compounds **16** & **17**. Results were analyzed to predict the structural requirements for the observed antitumor activity.

4. Experimental

4.1. Chemistry

^{1}H NMR spectra were run at 400 MHz and ^{13}C spectra were determined at 100 MHz in deuterated dimethyl sulfoxide (DMSO-d6) on a Varian Mercury VX-400 NMR spectrometer. Chemical shifts are given in parts per million (ppm) on the delta (ϒ) scale. Chemical shifts were calibrated relative to those of the solvents. The progress of reactions was monitored through thin-layer chromatography (TLC) using Merck silica gel IB2-F plates (0.25 mm thickness), where the spots were visualized through Vilber VL-6.LC UV lamp, with wavelength 365/ 254 nm. Mass spectra were recorded on a compact Mass Spectrometer (TLC-MS, Advion, USA) using APCI and ESI modes. Melting points were determined and were uncorrected, using capillary tubes with a Stuart SMP30 apparatus. All yields reported refer to isolated yields.

4-(4-Chlorophenyl)-1-thia-4-azaspiro [4.5] decan-3-one (2)

A solution of cyclohexanone (0.9 g, 10 mmol), *p*-chloro aniline (1.2 g, 10 mmol) and thioglycolic acid (0.9 g, 10 mmol) in dry toluene (50 ml) was refluxed for 10 h. the solution was concentrated, cooled to room temperature and the formed solid was filtered off, dried, and crystallized from ethanol to afford compound **2** as yellow solid, yield 87 %, m.p 131–132 °C; IR (KBr): ύ /cm^{-1}: 1675 (*C* = *O*); ^{1}H NMR (DMSO-*d6*) (ppm): 7.56 (d, *J* = 7.4 Hz, 2H), 7.23 (d, *J* = 7.4 Hz, 2H), 3.64 (s, 2H), 2.04–2.0 (m, 2H), 1.71–1.66 (m, 2H), 1.51–1.49 (m, 4H), 0.88–0.84 (m, 2H); MS (*m/z*): 281.

5′-Amino-3′-(4-chlorophenyl)-7′-(4-fluorophenyl)-3′H-spiro[cyclohexane-1,2′-thiazolo[4,5-b]pyridine]-6′-carbonitrile (3)

A mixture of **2** (2.8 g, 10 mmol), *p*-florobenzaldehyde (1.2 g, 10 mmol), ammonium acetate (1.5 g, 20 mmol) and malononitrile (0.6 g, 10 mmol) in glacial acetic acid (40 ml) was refluxed for 24 h. The reaction mixture was cooled to room temperature and poured onto water. The formed solid was filtrated off, dried, and crystallized from ethanol to afford compound **3** as yellow solid, yield 77 %, m.p 170–172 °C; IR (KBr): ύ /cm^{-1}: 3255 (NH_2), 2205 (CN); ^{1}H NMR (DMSO-*d6*) (ppm): 8.03 (d, *J* = 7.4 Hz, 2H), 7.61–7.52 (m, 4H), 7.32 (brs, 2H, D_2O exchangeable), 7.22 (d, *J* = 7.4 Hz, 2H), 2.01–1.96 (m, 2H), 1.70–1.66 (m, 2H), 1.52–1.48 (m, 4H), 0.88–0.81 (m, 2H); MS (*m/z*): 450.

3′-(4-Chlorophenyl)-9′-(4-fluorophenyl)-3′*H*-spiro[cyclohexane-1,2′-thiazolo[5′,4′:5,6]pyrido[2,3-d]pyrimidin]-8′(7′*H*)-one (4)

A solution of **3** (4.5 g, 10 mmol), formic acid (40 ml) was refluxed for 6 h, then cooled to room temperature and poured onto cold water. The formed precipitate was filtered off and recrystallized from ethanol to give compound **4** as brown crystals (69 %) mp = 168–169 °C; IR (KBr) cm^{-1}: 3350 (NH), 1672 (*C* = *O*); ^{1}H NMR (DMSO-*d6*) (ppm): 11.75 (brs, 1H, D_2O exchangeable), 8.49 (s, 1H), 7.52 (d, *J* = 7.4 Hz, 2H), 7.41–7.33 (m, 4H), 7.21 (d, *J* = 7.4 Hz, 2H), 2.01–1.96 (m, 2H), 1.70–1.64 (m, 2H), 1.49–1.44 (m, 4H), 0.90–0.84 (m, 2H); ^{13}C NMR (DMSO-d_6) δ: 166.1, 162.5, 159.5, 157.6, 153.6, 142.5, 139.4, 132.1, 129.5, 128.5, 127.8, 127.2, 127.1, 120.1, 115.3, 60.0, 43.9, 24.8, 18.6; MS (*m/z*) 478; Anal. Calc. for: ($C_{25}H_{20}ClFN_4OS$): C, 62.69; H, 4.21; N, 11.70 %; Found: C, 62.76; H, 4.27; N, 11.76 %.

3′-(4-Chlorophenyl)-9′-(4-fluorophenyl)-6′-methylspiro[cyclohexane-1,2′-thiazolo[5′,4′:5,6]pyrido[2,3-d] [1,3]oxazin]-8′(3′*H*)-one

Table 3
The binding mode and C-Docker interaction energy of the most potent newly synthesized compounds (**16** & **17**) compared to Roscovitine ligand.

Compound name	Binding mode	(-)C-Docker interaction energy (kcal/mol)	Key Amino acids/ interaction
Lead Compound Roscovitine	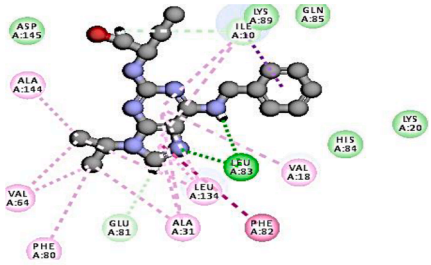	55.75	1 HBA with Leu83 1HBD with Leu83. Hydrophobic binding with ILE10, VAL18,ALA31,LYS33, VAL64,PHE80, PHE82, LYS89, LEU134 & ALA144
16	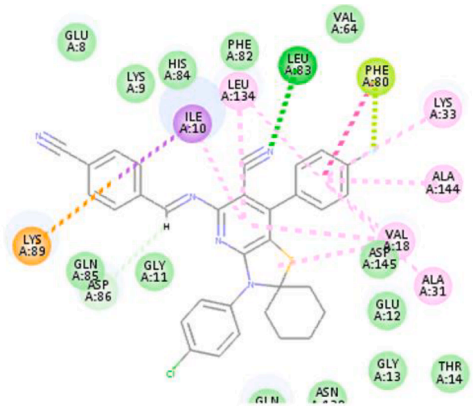	56.52	1 HBA with Leu83 Hydrophobic binding with ILE10, VAL18,ALA31,LYS33, PHE80, LEU134 & ALA144 Pi-cation interaction with LYS89 Carbon Hydrogen Bond with ASP86
17	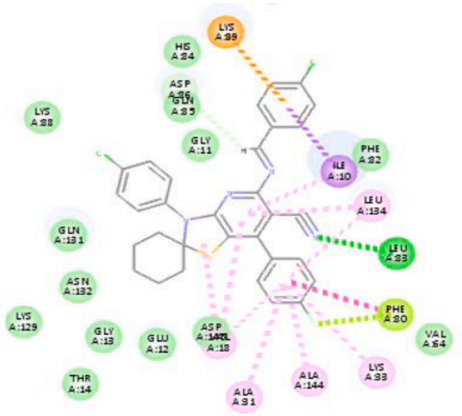	52.68	1 HBA with Leu83 Hydrophobic binding with ILE10, VAL18,ALA31,LYS33, PHE80, LEU134 & ALA144 Pi-cation interaction with LYS89 Carbon Hydrogen Bond with ASP86

(5)

A solution of **3** (4.5 g, 10 mmol) in acetic anhydride (10 ml) was heated under reflux for 5 h, the reaction mixture was cooled and poured over crushed ice, the formed precipitate was filtered off, washed with water and recrystallized from ethanol to give compound **5** as brown crystals (64 %) mp = 188–190 °C; IR (KBr) cm^{-1}: 1730 (*C* = *O*); ^{1}H NMR (DMSO-*d6*) (ppm): 7.51 (d, *J* = 7.4 Hz, 2H), 7.43–7.33 (m, 4H), 7.20 (d, *J* = 7.4 Hz, 2H), 2.02–1.96 (m, 2H), 1.68–1.65 (m, 2H), 1.48–1.46 (m, 4H), 1.08 (s, 3H), 0.84–0.82 (m, 2H); ^{13}C NMR (DMSO-d_6) δ: 166.1, 162.5, 159.4, 157.3, 153.5, 142.5, 139.4, 132.1, 129.5, 128.5, 127.8, 127.2, 127.1, 120.1, 114.9, 59.1, 43.9, 24.5, 21.1, 18.6; MS (*m/z*) 493; Anal. Calc. for: ($C_{26}H_{21}ClFN_3O_2S$): C, 63.22; H, 4.29; N, 8.51 %; Found: C, 63.28; H, 4.33; N, 8.56 %.

General procedure for compound 6 and 7:

A mixture of **3** (4.5 g, 10 mmol) and either urea (5 mmol; 0.3 g) or thiourea (5 mmol; 0.4 g) was fused at 280 °C using a sand bath for 1 h. The reaction mixture was cooled then triturated with ethanol. The obtained solid was filtered, washed several times with water, dried and recrystallized from dimethylformamide/water.

8′-Amino-3′-(4-chlorophenyl)-9′-(4-fluorophenyl)-3′*H*-spiro[cyclohexane-1,2′-thiazolo[5′,4′:5,6]pyrido[2,3-d]pyrimidin]-6′(5′*H*)-one (6)

Yellow crystals (71 %) mp = 198–200 °C; IR (KBr) cm^{-1}: 3330, 3227 (NH, NH_2), 1667 (*C* = *O*); ^{1}H NMR (DMSO-*d6*) (ppm): 9.54 (brs, 1H, D_2O exchangeable), 7.52 (d, *J* = 7.4 Hz, 2H), 7.39–7.31 (m, 4H), 7.21 (d, *J* = 7.4 Hz, 2H), 5.76 (brs, 2H, D_2O exchangeable), 2.0–1.98 (m, 2H), 1.71–1.67 (m, 2H), 1.48–1.44 (m, 4H), 0.84–0.80 (m, 2H); ^{13}C NMR (DMSO-d_6) δ: 166.1, 162.6, 161.1, 159.7, 153.5, 142.5, 139.4, 132.1, 129.5, 128.5, 127.8, 127.19, 127.12, 120.1, 114.9, 60.0, 44.8, 24.8, 18.6; MS (*m/z*) 493; Anal. Calc. for: ($C_{25}H_{21}ClFN_5OS$): C, 60.79; H, 4.29; N, 14.18 %; Found: C, 60.83; H, 4.33; N, 14.23 %.

8′-Amino-3′-(4-chlorophenyl)-9′-(4-fluorophenyl)-3′*H*-spiro[cyclohexane-1,2′-thiazolo[5′,4′:5,6]pyrido[2,3-d]pyrimidine]-6′(5′*H*)-thione (7)

Brown crystals (64 %) mp = 196–198 °C; IR (KBr) cm^{-1}: 3328, 3210 (NH, NH_2); ^{1}H NMR (DMSO-*d6*) (ppm): 13.48 (brs, 1H, D_2O exchangeable), 7.57 (d, *J* = 7.4 Hz, 2H), 7.39–7.28 (m, 4H), 7.23 (d, *J* = 7.4 Hz, 2H), 6.33 (brs, 2H, D_2O exchangeable), 2.01–1.96 (m, 2H), 1.69–1.64 (m, 2H), 1.48–1.44 (m, 4H), 0.85–0.83 (m, 2H); ^{13}C NMR

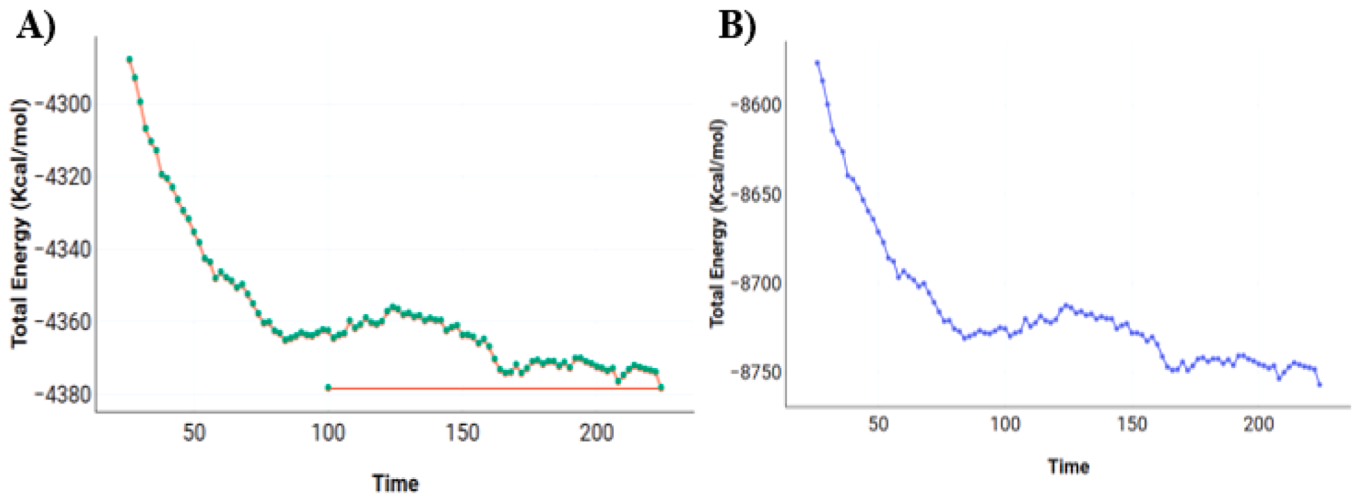

Fig. 7. A) Total Energy versus time overlay for compound **16 (green) & 17 (red),** versus **B)** the free CDK2 protein in **blue.**

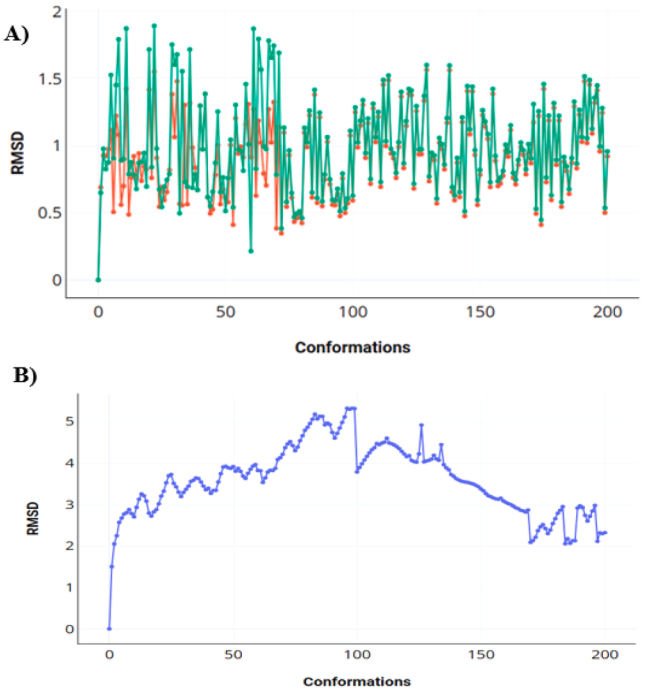

Fig. 8. RMSD for **A)** compound **16 (green), 17(red)**, versus **B)** the CDK2 protein itself in **blue.**

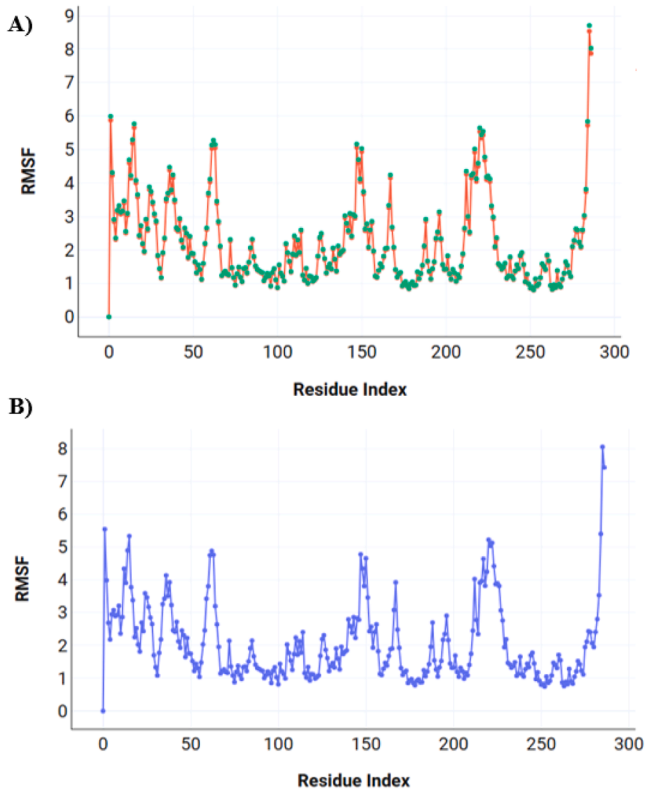

Fig. 9. RMSF A)for compound 16**(green)** & 17**(red)**, versus **B)** the protein CDK2 itself in **blue.**

(DMSO-d_6) δ: 180.2, 166.1, 162.5, 161.5, 153.5, 142.5, 139.4, 132.1, 129.5, 129.4, 128.5, 127.8, 127.1, 120.2, 115.1, 59.9, 43.7, 24.5, 18.6; MS (*m/z*) 510; Anal. Calc. for: ($C_{25}H_{21}ClFN_5S_2$): C, 58.87; H, 4.15; N, 13.73 %; Found: C, 58.94; H, 4.21; N, 13.81 %.

3′-(4-Chlorophenyl)-9′-(4-fluorophenyl)-6′-phenylspiro[cyclohexane-1,2′-thiazolo[5′,4′:5,6]pyrido[2,3-d] [1,3]oxazin]-8′(3′H)-one (8)

A mixture of **3** (4.5 g, 10 mmol) and benzoyl chloride (5 ml) was refluxed in pyridine (20 ml) for 6 h. The excess of the benzoyl chloride was removed by distillation under vacuum, and the residue was cooled and added to ice/water. The precipitate thus obtained was collected, dried and recrystallized from ethanol to give compound **8** as yellow crystals (77 %) mp = 178–180 °C; IR (KBr) cm^{-1}: 1742 (*C = O*); ^{1}H NMR (DMSO-*d6*) (ppm): 7.95 (d, *J* = 12 Hz, 2H), 7.74 (d, *J* = 12 Hz, 2H), 7.52 (d, *J* = 7.4 Hz, 2H), 7.43 (d, *J* = 8 Hz, 2H), 7.34–7.26 (m, 4H), 7.20 (d, *J* = 7.4 Hz, 2H), 2.0–1.95 (m, 2H), 1.67–1.66 (m, 2H), 1.48–1.46 (m, 4H), 0.84–0.81 (m, 2H); ^{13}C NMR (DMSO-d_6) δ: 166.2, 159.9, 159.2, 157.9, 153.8, 150.0, 147.3, 142.5, 139.4, 132.1, 132.0, 129.5, 128.5, 127.8, 127.2, 127.1, 119.9, 117.1, 115.0, 60.0, 43.7, 24.7, 18.7; MS (*m/z*) 556; Anal. Calc. for: ($C_{31}H_{23}ClFN_3O_2S$): C, 66.96; H, 4.17; N, 7.56 %; Found: C, 67.02; H, 4.24; N, 7.61 %.

3′-(4-Chlorophenyl)-9′-(4-fluorophenyl)-3′H-spiro[cyclohexane-1,2′-thiazolo[5′,4′:5,6]pyrido[2,3-d]pyrimidin]-8′-amine (9)

A mixture of **3** (4.5 g, 10 mmol) and formamide (20 ml) was refluxed for 20 h. The reaction mixture was cooled, poured onto ice/water, and the solid product that appeared was collected by filtration and recrystallized from ethanol to give compound **9** as brown crystals (69 %) mp = 252–254 °C; IR (KBr) cm^{-1}: 3329 (NH_2); ^{1}H NMR (DMSO-*d6*) (ppm):

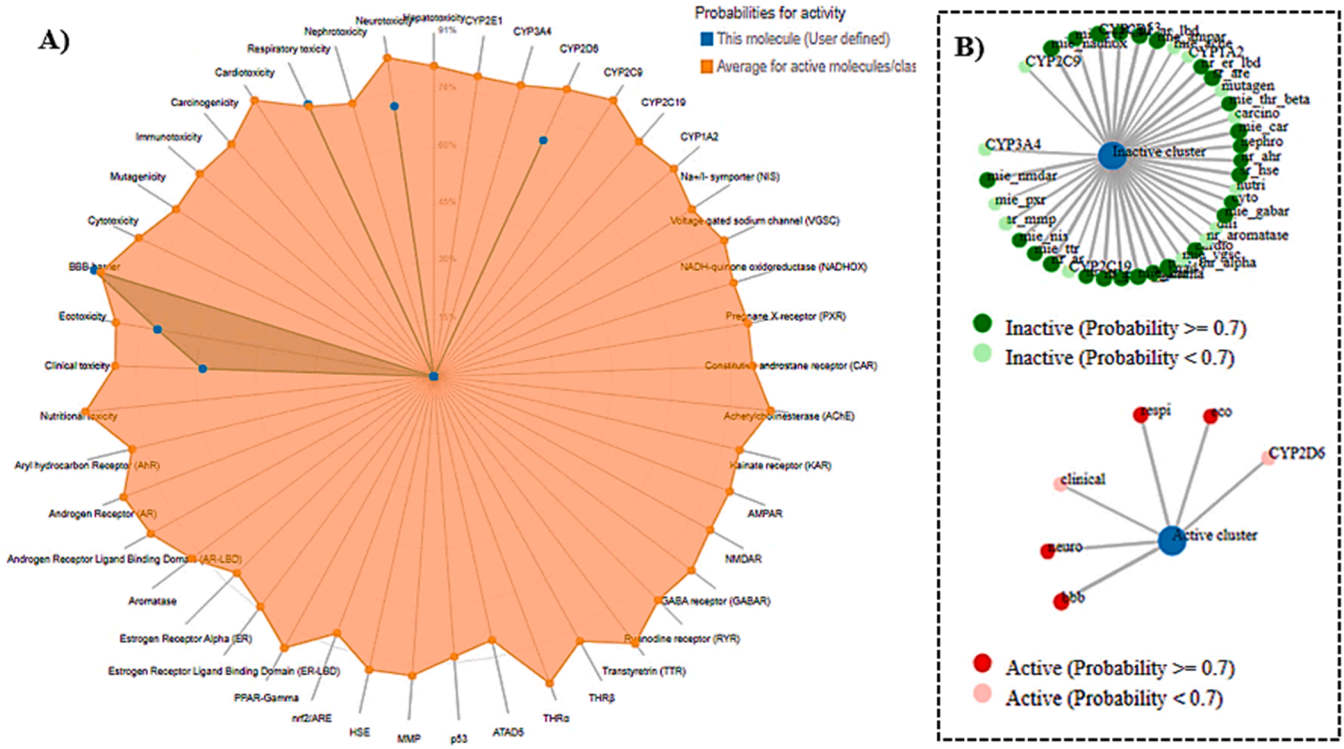

Fig. 10. Toxicity Prediction results using ProTox for compounds **16** & **17 A)** Toxicity Radar Chart representing the probable toxicity points (as blue points), **B)** Network chart with predicted activities.

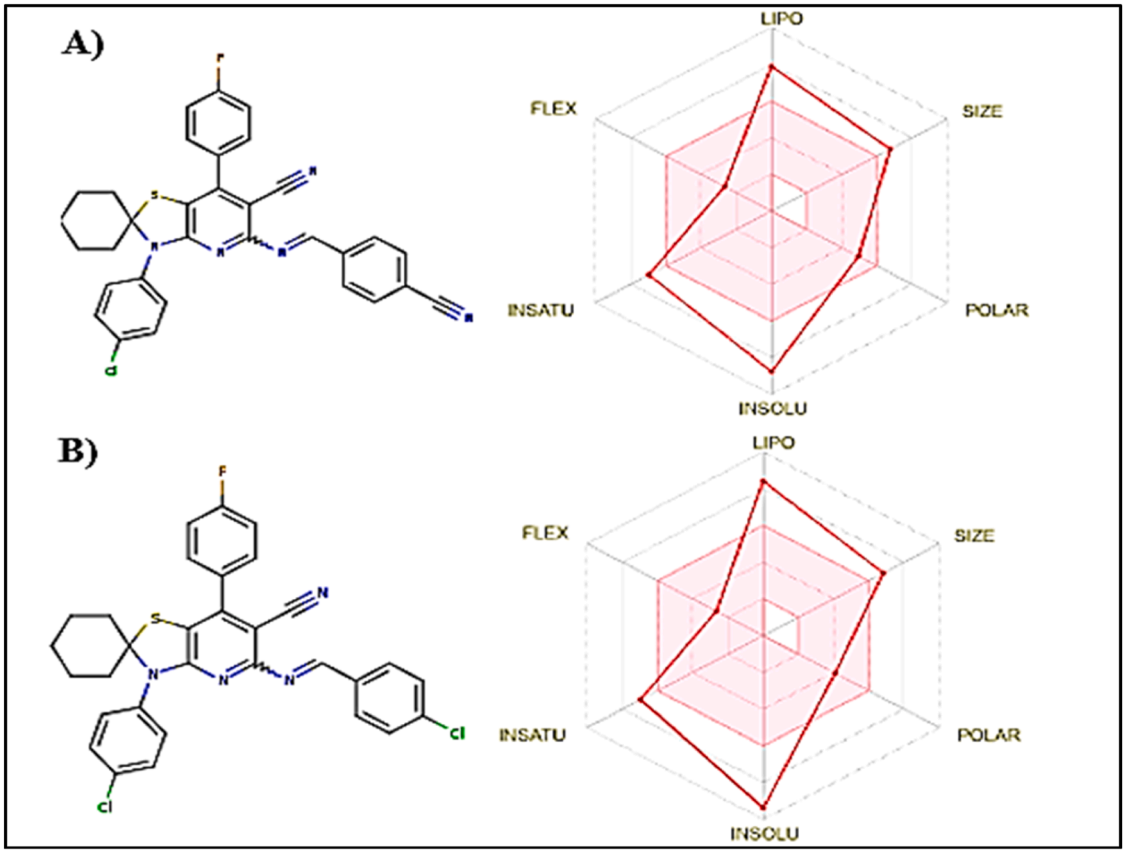

Fig. 11. The bioavailability radar chart of compounds **A)** compound **16** & **B)** compound **17**.

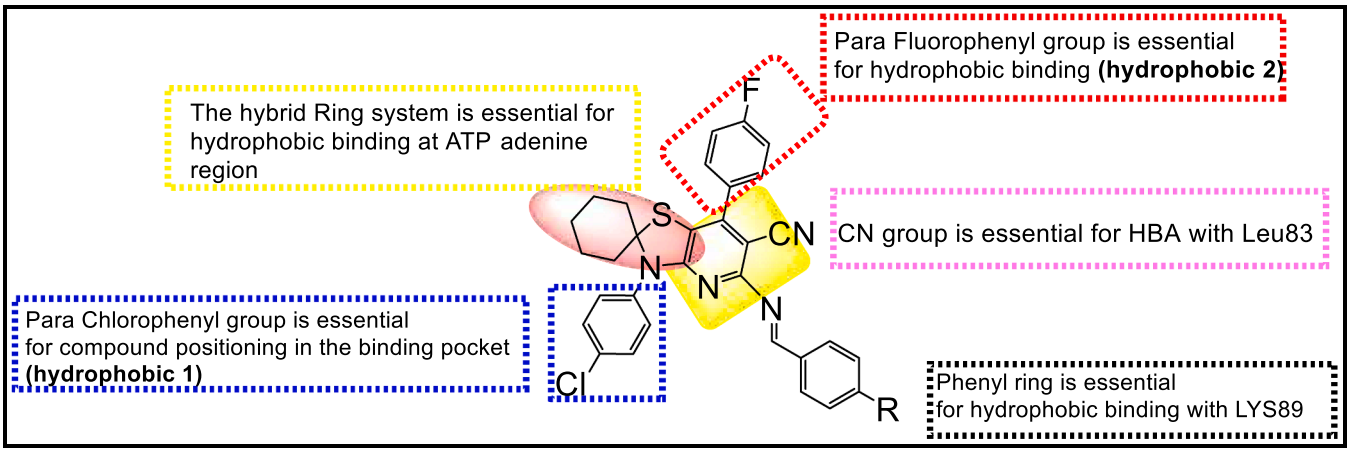

Fig. 12. Structure activity relationship **(SAR)** for the two promising compounds **(16–17)**.

8.54 (s, 1H), 7.54 (d, $J = 7.4$ Hz, 2H), 7.40–7.29 (m, 4H), 7.23 (d, $J = 7.4$ Hz, 2H), 6.57 (brs, 2H, D_2O exchangeable), 2.01–1.98 (m, 2H), 1.69–1.66 (m, 2H), 1.56–1.49 (m, 4H), 0.89–0.81 (m, 2H); ^{13}C NMR (DMSO-d_6) δ: 166.2, 163.9, 160.2, 157.8, 153.8, 142.5, 139.4, 132.1, 129.5, 128.5, 128.8, 127.2, 127.1, 119.6, 115.1, 60.2, 43.9, 24.4, 18.7; MS (*m/z*) 477; Anal. Calc. for: ($C_{25}H_{21}ClFN_5S$): C, 62.82; H, 4.43; N, 14.65 %; Found: C, 62.87; H, 4.47; N, 14.68 %.

5′-Amino-3′-(4-chlorophenyl)-7′-(4-fluorophenyl)-3′*H*-spiro[cyclohexane-1,2′-thiazolo[4,5-b]pyridine]-6′-carboxamide (10)

A sample of **3** (4.5 g, 10 mmol) was warmed in 60 % aqueous H_2SO_4 (10 ml) with stirring for 0.5 h. The reaction mixture was cooled, diluted with cold water, and then neutralized (pH 8) by addition of aqueous sodium hydroxide solution (10 %). The resulting precipitate was recrystallized from ethanol to give the carboxamide derivative **10** as yellow crystals (66 %) mp = 189–1190 °C; IR (KBr) cm^{-1}: 3333 (NH_2), 1682 (*C = O*); ^{1}H NMR (DMSO-*d6*) (ppm): 8.68 (brs, 2H, D_2O exchangeable), 7.62 (d, $J = 7.4$ Hz, 2H), 7.54 (d, $J = 8$ Hz, 2H), 7.38 (d, $J = 7.4$ Hz, 2H), 7.25 (d, $J = 8$ Hz, 2H), 6.20 (brs, 2H, D_2O exchangeable), 2.01–1.98 (m, 2H), 1.68–1.67 (m, 2H), 1.52–1.49 (m, 4H), 0.88–0.81 (m, 2H); ^{13}C NMR (DMSO-d_6) δ: 166.1, 162.4, 159.5, 153.6, 142.5, 139.4, 132.1, 129.5, 128.5, 127.9, 127.18, 127.13, 119.9, 115.1, 60.1, 43.8, 24.5, 18.6; MS (*m/z*) 468; Anal. Calc. for: ($C_{24}H_{22}ClFN_4OS$): C, 61.47; H, 4.73; N, 11.95 %; Found: C, 61.51; H, 4.77; N, 11.99 %.

Ethyl(*E*)-*N*-(3′-(4-chlorophenyl)-6′-cyano-7′-(4-fluorophenyl)-3′*H*-spiro[cyclohexane-1,2′-thiazolo[4,5-b]pyridin]-5′-yl)formimidate (11)

A mixture of **3** (4.5 g, 10 mmol) and triethyl orthoformate (10 ml) was refluxed for 6 h. The reaction mixture was cooled and the solid product that appeared was collected by filtration and recrystallized from ethanol to give compound **11** as brown crystals (78 %) mp = 207–209 °C; IR (KBr) cm^{-1}: 2229 (CN); ^{1}H NMR (DMSO-*d6*) (ppm): 8.02 (s, 1H), 7.53 (d, $J = 7.4$ Hz, 2H), 7.38–7.33 (m, 4H), 7.22 (d, $J = 7.4$ Hz, 2H), 3.67 (q, $J = 12$ Hz, 2H), 1.99–1.96 (m, 2H), 1.66–1.64 (m, 2H), 1.51–1.46 (m, 4H), 1.11 (d, $J = 12$ Hz, 3H), 0.86–0.81 (m, 2H); ^{13}C NMR (DMSO-d_6) δ: 161.9, 159.2, 157.2, 153.4, 142.5, 139.4, 132.1, 129.5, 128.5, 127.8, 127.2, 127.18, 127.13, 120.0, 115.1, 65.4, 60.0, 43.8, 24.2, 18.6, 15.3; MS (*m/z*) 507; Anal. Calc. for: ($C_{27}H_{24}ClFN_4OS$): C, 63.96; H, 4.77; N, 11.05 %; Found: C, 64.02; H, 4.82; N, 11.09 %.

General procedure for compounds 12, 13 and 14:

A mixture of **3** (4.5 g, 10 mmol), the aldose sugars namely, D-glucose or D-galactose, or D-xylose (0.01 mol) and glacial acetic acid (1 ml) in ethanol (40 ml) was refluxed for 7–9 h. The solution was concentrated then cooled to room temperature and poured into ice cooled water. The resulting precipitated solid was filtered, dried, and recrystallized from methanol to afford compounds **12** ,**13** and **14**, respectively.

3′-(4-Chlorophenyl)-7′-(4-fluorophenyl)-5′-(((2*S*,3*R*,4*R*,5*R*,*E*)-2,3,4,5,6-pentahydroxyhexylidene)amino)-3′*H*-spiro[cyclohexane-1,2′-thiazolo[4,5-b]pyridine]-6′-carbonitrile (12)

Yellow crystals (72 %) mp = 212–214 °C; IR (KBr) cm^{-1}: 3410 (OH), 2210 (CN); ^{1}H NMR (DMSO-*d6*) (ppm): 10.32 (m, 1H), 7.52 (d, $J = 7.4$ Hz, 2H), 7.39–7.29 (m, 4H), 7.21 (d, $J = 7.4$ Hz, 2H), 6.27 (brs, 1H, D_2O exchangeable), 5.57 (brs, 1H, D_2O exchangeable), 4.95 (brs, 2H, D_2O exchangeable), 4.36 (brs, 1H, D_2O exchangeable), 3.76–3.70 (m, 4H), 3.64–3.61 (m, 2H), 1.98–1.96 (m, 2H), 1.69–1.66 (m, 2H), 1.48–1.46 (m, 4H), 0.89–0.84 (m, 2H); ^{13}C NMR (DMSO-d_6) δ: 166.2, 163.6, 159.6, 153.5, 142.5, 139.4, 132.2, 129.5, 128.5, 127.8, 127.17, 127.11, 119.9, 117.9, 115.3, 74.9, 71.1, 68.0, 64.8, 62.8, 59.6, 43.8, 24.9, 18.6; MS (*m/z*) 613; Anal. Calc. for: ($C_{30}H_{30}ClFN_4O_5S$): C, 58.77; H, 4.93; N, 9.14 %; Found: C, 58.83; H, 4.99; N, 9.19 %.

3′-(4-Chlorophenyl)-7′-(4-fluorophenyl)-5′-(((2*S*,3*R*,4*S*,5*R*,*E*)-2,3,4,5,6-pentahydroxyhexylidene)amino)-3′*H*-spiro[cyclohexane-1,2′-thiazolo[4,5-b]pyridine]-6′-carbonitrile (13)

Yellow crystals (69 %) mp = 205–207 °C; IR (KBr) cm^{-1}: 3413 (OH), 2210 (CN); ^{1}H NMR (DMSO-*d6*) (ppm): 10.31 (m, 1H), 7.53 (d, $J = 7.4$ Hz, 2H), 7.41–7.33 (m, 4H), 7.21 (d, $J = 7.4$ Hz, 2H), 6.28 (brs, 1H, D_2O exchangeable), 5.58 (brs, 1H, D_2O exchangeable), 4.99 (brs, 2H, D_2O exchangeable), 4.36 (brs, 1H, D_2O exchangeable), 3.77–3.68 (m, 4H), 3.57–3.52 (m, 2H), 2.03–1.98 (m, 2H), 1.68–1.63 (m, 2H), 1.52–1.48 (m, 4H), 0.85–0.84 (m, 2H); ^{13}C NMR (DMSO-d_6) δ: 166.1, 163.6, 159.4, 153.5, 142.5, 139.4, 132.2, 129.5, 128.5, 127.8, 127.17, 127.11, 119.9, 117.9, 115.3, 74.9, 71.1, 68.0, 64.8, 62.8, 59.6, 43.8, 24.9, 18.6; MS (*m/z*) 613; Anal. Calc. for: ($C_{30}H_{30}ClFN_4O_5S$): C, 58.77; H, 4.93; N, 9.14 %; Found: C, 58.81; H, 4.97; N, 9.17 %.

3′-(4-Chlorophenyl)-7′-(4-fluorophenyl)-5′-(((2*S*,3*R*,4*R*,*E*)-2,3,4,5-tetrahydroxypentylidene)amino)-3′*H*-spiro[cyclohexane-1,2′-thiazolo[4,5-b]pyridine]-6′-carbonitrile (14)

Yellow crystals (65 %) mp = 215–217 °C; IR (KBr) cm^{-1}: 3433 (OH), 2218 (CN); ^{1}H NMR (DMSO-*d6*) (ppm): 10.24 (m, 1H), 7.52 (d, $J = 7.4$ Hz, 2H), 7.41–7.30 (m, 4H), 7.19 (d, $J = 7.4$ Hz, 2H), 5.59 (brs, 1H, D_2O exchangeable), 5.0 (brs, 2H, D_2O exchangeable), 4.44 (brs, 1H, D_2O exchangeable), 3.68–3.58 (m, 5H), 1.98–1.96 (m, 2H), 1.66–1.64 (m, 2H), 1.48–1.46 (m, 4H), 0.84–0.83 (m, 2H); ^{13}C NMR (DMSO-d_6) δ: 166.1, 162.3, 159.3, 153.6, 142.5, 139.4, 132.1, 129.5, 128.5, 127.8, 127.2, 126.9, 119.9, 117.4, 115.0, 75.1, 70.1, 66.4, 63.2, 60.6, 43.9, 24.0, 18.3; MS (*m/z*) 583; Anal. Calc. for: ($C_{29}H_{28}ClFN_4O_4S$): C, 59.74; H, 4.84; N, 9.61 %; Found: C, 59.79; H, 4.91; N, 9.68 %.

General procedure for compound 15, 16 and 17:

A mixture of **3** (4.5 g, 10 mmol), aromatic aldehyde derivatives namely, *p*-nitro benzaldehyde, or *p*-cyanobenzaldehyde, or *p*-chlorobenzaldehyde (0.01 mol) and glacial acetic acid (1 ml) in ethanol (40 ml) was refluxed for 7–8 h. The solution was concentrated then poured onto ice water and the formed solid was filtered, dried, and recrystallized from methanol to afford the compounds **11, 12** and **13** respectively.

(*E*)-3′-(4-Chlorophenyl)-7′-(4-fluorophenyl)-5′-((4-nitrobenzylidene)

amino)-3′*H*-spiro[cyclohexane-1,2′-thiazolo[4,5-b]pyridine]-6′-carbonitrile (15)

Red crystals (65 %) mp =238–240 °C; IR (KBr) cm^{-1}: 2222 (CN); ^{1}H NMR (DMSO-*d6*) (ppm): 10.12 (s, 1H), 7.92 (d, *J* = 8 Hz, 2H), 7.72 (d, *J* = 8 Hz, 2H), 7.54 (d, *J* = 7.4 Hz, 2H), 7.46–7.31 (m, 4H), 7.24 (d, *J* = 7.4 Hz, 2H), 2.01–1.96 (m, 2H), 1.71–1.68 (m, 2H), 1.51–1.47 (m, 4H), 0.91–0.85 (m, 2H); ^{13}C NMR (DMSO-d_6) δ: 162.5, 159.5, 158.1, 153.6, 150.2, 147.9, 142.5, 139.4, 132.1, 129.5, 128.5, 127.8, 127.2, 127.1, 121.8, 119.8, 114.8, 106.7, 59.7, 44.8, 24.9, 18.6; MS (*m/z*) 584; Anal. Calc. for: ($C_{31}H_{23}ClFN_5O_2S$): C, 63.75; H, 3.97; N, 11.99 %; Found: C, 63.81; H, 4.01; N, 12.03 %.

(*E*)-3′-(4-Chlorophenyl)-5′-((4-cyanobenzylidene)amino)-7′-(4-fluorophenyl)-3′*H*-spiro[cyclohexane-1,2′-thiazolo[4,5-b]pyridine]-6′-carbonitrile (16)

Brown crystals (65 %) mp = 240–242 °C; IR (KBr) cm^{-1}: 2222 (CN); ^{1}H NMR (DMSO-*d6*) (ppm): 10.10 (s, 1H), 8.08 (d, *J* = 8 Hz, 2H), 7.81 (d, *J* = 8 Hz, 2H), 7.54 (d, *J* = 7.4 Hz, 2H), 7.42–7.34 (m, 4H), 7.34 (d, *J* = 7.4 Hz, 2H), 2.01–1.98 (m, 2H), 1.71–1.69 (m, 2H), 1.52–1.49 (m, 4H), 0.91–0.87 (m, 2H); ^{13}C NMR (DMSO-d_6) δ: 166.1, 162.7, 159.4, 153.2, 150.0, 147.4, 142.5, 139.4, 132.1, 129.5, 128.5, 127.9, 127.18, 127.11, 121.0, 119.8, 116.9, 114.9, 106.5, 59.8, 43.9, 24.7, 18.6; MS (*m/z*) 564; Anal. Calc. for: ($C_{32}H_{23}ClFN_5S$): C, 68.14; H, 4.11; N, 12.42 %; Found: C, 68.19; H, 4.15; N, 12.45 %.

(*E*)-5′-((4-Chlorobenzylidene)amino)-3′-(4-chlorophenyl)-7′-(4-fluorophenyl)-3′*H*-spiro[cyclohexane-1,2′-thiazolo[4,5-b]pyridine]-6′-carbonitrile (17)

Brown crystals (65 %) mp = 227–229 °C; IR (KBr) cm^{-1}: 2222 (CN); ^{1}H NMR (DMSO-*d6*) (ppm): 10.11 (s, 1H), 7.97 (d, *J* = 8 Hz, 2H), 7.72 (d, *J* = 8 Hz, 2H), 7.52 (d, *J* = 7.4 Hz, 2H), 7.46–7.32 (m, 4H), 7.34 (d, *J* = 7.4 Hz, 2H), 2.01–1.96 (m, 2H), 1.71–1.68 (m, 2H), 1.52–1.47 (m, 4H), 0.91–0.85 (m, 2H); ^{13}C NMR (DMSO-d_6) δ: 166.2, 162.5, 159.1, 153.6, 149.9, 146.8, 142.5, 139.4, 132.1, 129.5, 128.5, 127.8, 127.2, 127.1, 120.1, 117.4, 114.9, 106.0, 60.1, 44.8, 23.9, 18.7; MS (*m/z*) 573; Anal. Calc. for: ($C_{31}H_{23}Cl_2FN_4S$): C, 64.92; H, 4.04; N, 9.77 %; Found: C, 64.97; H, 4.09; N, 10.02 %.

4.2. Biological assays

4.2.1. In vitro anti-proliferative activity

The in vitro cytotoxic activity of the synthesized compounds was evaluated against two human cancer cell lines: A549 (lung adenocarcinoma) and MCF-7 (breast adenocarcinoma). The anticancer drug Sorafenib was used as a reference standard for comparison.

Cell lines were cultured under aseptic conditions in RPMI-1640 medium (Gibco, NY, USA), supplemented with 10 % fetal bovine serum (FBS) (Biocell, CA, USA), and maintained at 37 °C in a humidified incubator with 5 % CO_2 atmosphere.

To assess anti-proliferative activity, a cell suspension of 5×10^5 cells/mL was prepared. Each test compound was initially dissolved in dimethyl sulfoxide (DMSO) and further diluted with phosphate-buffered saline (PBS) to obtain final concentrations ranging from 0.01 to 100 μM, ensuring that the final DMSO concentration did not exceed 1 % in any well.

Aliquots of 0.2 mL of each compound concentration were added in duplicate to individual wells of a sterile microtiter plate. Then, 1.8 mL of the prepared cell suspension (6×10^4 cells/mL) was added to each well, making up a final volume of 2.0 mL per well. Negative controls containing only PBS and 1 % DMSO and positive control wells containing Sorafenib were included for comparison.

After 48 h of incubation, the contents of each well were diluted 1:10 with sterile saline, and viable cell counts were determined using a Coulter counter. Cell counts were corrected for dilution, and IC_{50} values were calculated relative to the untreated control wells [45].

4.2.2. CDK2/ cyclin A2 assay

The in vitro assay of CDK2/ cyclin A2 protein kinase was carried out on all of the synthesized compounds. Kinase assay was performed in 96-well white plate in a 50 μL volume reaction. The reaction was performed in four steps in the following order: 2.5 μL of the test compounds or 5 % DMSO, 5 μL of CDK2/Cyclin A2 enzyme (1.6 ng) was added and then incubated at room temperature for 30 min. Then 5 μL of (50 μM ATP. 0.1 μg/μL Histone H1 was added and incubated for 10 min. The reaction was stopped by adding 12.5 μL of ADP-Glo™ Reagent and incubated for 40 min. 25 μL of kinase detection reagent was added to each well and incubated for 60 min before detection with luminescence (Integration time 0.5-1 s) [46–48].

4.3. In silico studies

4.3.1. Molecular modeling studies

Molecular docking study was carried out using Discovery Studio 4.0 Software. The X-ray crystallographic structure of CDK2 complexed with Roscovitine (PDB ID: 2A4L) was downloaded from PDB [49,50]. Molecular simulations was proceeded using C-Docker protocol on the tested compounds. Protein was cleaned; missing residues were completed and Hydrogen atom was added. All the unnecessary radicals in addition to water molecules were also removed. Force Field simulation using CHARMm with partial charge of MMFF94 were applied [42]. The target was successfully prepared and minimized before the active site was identified using ligand selection. The downloaded ligand was removed and re-docked with the prepared tested compounds.

Visual inspection was applied to predict the best pose out of ten for each docked compound as compared to the ligand binding mode.

4.3.2. Dynamic simulation

The dynamic simulation studies were carried out using Discovery Studio 4.0 and applied to the free CDK2 protein (PDB ID: 2A4L) in complex with the two selected compounds **(**compound **16** and compound **17)** that demonstrated the highest binding affinity and stability in molecular docking. The Standard Dynamics Cascade protocol was used. The initial energy minimization step was conducted using the Steepest Descent algorithm with a maximum of 2000 steps and an RMS gradient of 1.0. This was followed by the Conjugate Gradient minimization, set to a maximum of 1000 steps. The initial temperature was adjusted to 50 °C**,** and the target temperature was set at 300 °C**,** with a maximum velocity of 2000. The equilibration phase was performed for 50 picoseconds (ps) with an interval of 2 ps**.**

The simulation was conducted using the Generalized Born with Simple Switching (GBSW) as the implicit solvent model**,** and the Leap-frog Verlet integrator was applied to propagate the dynamics of the system. The trajectories were analyzed to evaluate the total energy, RMSD (Root Mean Square Deviation)**,** and RMSF (Root Mean Square Fluctuation)**,** in order to determine the structural stability and flexibility of the CDK2-ligand complexes during the simulation period [51].

4.3.3. Toxicity prediction using protox 3.0 webserver

ProTox 3.0 is a machine-learning model recently applied to predict a total number of toxicity endpoints (61), between Acute Toxicity (45) and toxicity targets (16) with good reliable results. It includes: Organ Toxicity, Toxicity End Points, adverse outcomes (Tox21) pathways (Tox21-Nuclear Receptor Signaling Pathways, Tox21-Stress Response Pathways), Molecular-Initiating Events (MOE), and Metabolism with a detailed descriptor results [52–54].

Compounds **16** & **17** were fed to the server through SMILES (Simplified Molecular-Input Line Entry System) using SwissADME online tool [52].

4.3.4. In silico predictive ADME study

The pharmacokinetic profile of the two tested compounds (**16** & **17**) were determined using SwissADME online tool provided by the Swiss Institute of Bioinformatics [53,55]. The physicochemical characteristics of the tested compounds determine their suitability for biological

systems. The radar plot feature of SwissADME identifies the preferred ranges for six key features: polarity, size, solubility, lipophilicity, flexibility, and saturation. The software was employed to detect two essential pharmacokinetic parameters, the ability to cross blood-brain barrier and gastrointestinal tract (GIT) absorption.

Funding

This research did not receive any specific grant from funding agencies in the public, commercial, or not-for-profit sectors.

Author contribution

All authors have contributed in all the steps of building up the article and approved the final article.

Conflicts of interest

All the authors declare that they have no conflict of interest.

Data availability

Supporting data is available. Any further needed data are available from the corresponding author on request.

CRediT authorship contribution statement

Naglaa M. Anter: Writing – review & editing, Writing – original draft, Supervision, Methodology, Investigation, Conceptualization. **Asmaa A. Mandour:** Writing – review & editing, Writing – original draft, Visualization, Validation, Software, Methodology, Investigation, Formal analysis, Data curation. **Menna A. Ewida:** Writing – review & editing, Writing – original draft, Visualization, Validation, Software, Resources, Methodology, Data curation. **Ahmed F. El Farargy:** Writing – review & editing, Writing – original draft, Supervision, Resources, Project administration, Methodology, Funding acquisition, Formal analysis, Conceptualization. **Ibrahim F. Nassar:** Writing – original draft, Resources, Methodology, Investigation, Formal analysis, Data curation, Conceptualization. **Mohamed H. Sobhy:** Writing – original draft, Supervision, Resources, Project administration, Methodology, Investigation, Data curation, Conceptualization. **Abdelrahman A. Abuelkhir:** Visualization, Validation, Methodology, Investigation, Formal analysis, Data curation. **Hoda S. El Saeed:** Writing – review & editing, Writing – original draft, Visualization, Resources, Project administration, Data curation, Conceptualization. **Mohamed Hagras:** Writing – review & editing, Writing – original draft, Supervision, Project administration, Methodology, Investigation, Conceptualization. **Nasser S.M. Ismail:** Writing – review & editing, Writing – original draft, Visualization, Validation, Supervision, Project administration, Methodology, Data curation, Conceptualization.

Declaration of competing interest

All the authors declare that there is no conflict of interest.

Acknowledgements

Acknowledgement for Ain Shams University for performing molecular modeling study in Computer Aided Drug Design labs. The cell lines were obtained from Texas University Health Sciences Center (by Associate Professor: Heba A.Ewida)

Data availability

Data will be made available on request.

References

[1] J. Chen, X. Wang, J.Z. Zhang, T. Zhu, ACS Omega 3 (2018) 18052–18064.
[2] A.A. Abdel-Rahman, A.K. Shaban, I.F. Nassar, D.S. El-Kady, N.S. Ismail, S. F. Mahmoud, H.M. Awad, W.A. El-Sayed, Molecules 26 (2021) 3923.
[3] J. Chen, L. Pang, W. Wang, L. Wang, J.Z. Zhang, T. Zhu, J. Biomol. Struct. Dyn. 38 (2020) 985–996.
[4] J. Chen, X. Wang, J.Z. Zhang, T. Zhu, ACS Omega 3 (2018) 18052–18064.
[5] G. Kontopidis, C. McInnes, S.R. Pandalaneni, I. McNae, D. Gibson, M. Mezna, M. Thomas, G. Wood, S. Wang, M.D. Walkinshaw, P.M. Fischer, Chem. Biol. 13 (2006) 201–211.
[6] N.E.A. Abd El-sattar, E.H.K. Badawy, W.H. AbdEl-Hady, M.I. Abo-Alkasem, A. A. Mandour, N.S.M. Ismail, Chem. Pharm. Bull. 69 (2021) 106–117.
[7] D.O. Morgan, Nature 374 (1995) 131–134.
[8] S. Ortega, M. Malumbres, M. Barbacid, Biochim. Biophys. Acta 1602 (2002) 73–87.
[9] C.L. Braal, E.M. Jongbloed, S.M. Wilting, R.H. Mathijssen, S.L. Koolen, A. Jager, Drugs 81 (2021) 317–331.
[10] M. Malumbres, M. Barbacid, Nat. Rev. Cancer 9 (2009) 153–166.
[11] D. Santamaría, C. Barriere, A. Cerqueira, S. Hunt, C. Tardy, K. Newton, J. F. Cáceres, P. Dubus, M. Malumbres, M. Barbacid, Nature 448 (2007) 811–815.
[12] S. Fortin, G. Berube, Expert Opin. Drug Discov. 8 (2013) 1029–1047.
[13] W.A. El-Sayed, H.S. Khalaf, S.F. Mohamed, H.A. Hussien, O.M. Kutkat, A.E. Amr, Russ. J. Gen. Chem. 87 (2017) 2444–2453.
[14] A.M. Mohamed, H.R.M. Al-Qalawi, W.A. El-Sayed, W.A.A. Arafa, Acta Pol. Pharm. 72 (2015) 307–318.
[15] H.S. Khalaf, H.E. Tolana, M.N. El-Bayaaa, M.A. Radwan, M. El-Manawaty, W.A. El-Sayed, Russ. J. Gen. Chem. 90 (2020) 1706–1715.
[16] S. Prachayasittikul, R. Pingaew, A. Worachartcheewan, N. Sinthupoom, V. Prachayasittikul, S. Ruchirawat, V. Prachayasittikul, Mini Rev. Med. Chem. 17 (2017) 869–901.
[17] A.E. Rashad, A.E Mahmoud, M.M. Ali, Eur. J. Med. Chem. 46 (2011) 1019–1026.
[18] S. Schenone, F.Bondavalli O.Bruno, A. Ranise, L. Mosti, G. Menozzi, P. Fossa, S. Donnini, A. Santoro, M. Ziche, F. Manetti, Eur. J. Med. Chem. 39 (2004) 939–946.
[19] I. Devesa, M.J. Alcaraz, R. Riguera, M.L. Ferrándiz, Eur. J. Pharmacol. 488 (2004) 225–230.
[20] H.A.S. Abbas, W.A. El-Sayed, N.M. Fathy, Eur. J. Med. Chem. 45 (2010) 973–982.
[21] E. Abdel-Latif, S. Abdel-Fattah, H.E. Gaffer, H.A. Etman, Egypt. J. Basic Appl. Sci. 3 (2016) 118–124.
[22] S. Cherukupalli, R. Karpoormath, B. Chandrasekaran, G.A. Hampannavar, N. Thapliyal, V.N. Palakollu, Eur. J. Med. Chem. 126 (2017) 298–352.
[23] G.M. Ali, D.A. Ibrahim, A.M. Elmetwali, N.S. Ismail, Bioorg. Chem. 86 (2019) 1–4.
[24] A.M. Farag, A.M. Fahim, J. Mol. Struct. 1179 (2019) 304–314.
[25] N. Gökhan-Kelekçi, S. Yabanoğlu, E. Küpeli, U. Salgın, Ö. Özgen, G. Uçar, E. Yeşilada, E. Kendi, A. Yeşilada, A.A. Bilgin, Bioorg. Med. Chem. 15 (2007) 5775–5786.
[26] R. Nithyabalaji, H. Krishnan, R. Sribalan, J. Mol. Struct. 1186 (2019) 1–10.
[27] E. Hernández-Vázquez, S. Salgado-Barrera, J.J. Ramírez-Espinosa, S. Estrada-Soto, F. Hernández-Luis, Bioorg. Med. Chem. 24 (2016) 2298–2306.
[28] R.R. Pillai, K. Karrouchi, S. Fettach, S. Armaković, S.J. Armaković, Y. Brik, J. Taoufik, S. Radi, M.E. Faouzi, J. Mol. Struct. 1177 (2019) 47–54.
[29] E. Hernández-Vázquez, H. Ocampo-Montalban, L. Cerón-Romero, M. Cruz, J. Gómez-Zamudio, G. Hiriart-Valencia, R. Villalobos-Molina, A. Flores-Flores, S. Estrada-Soto, Eur. J. Pharmacol. 803 (2017) 159–166.
[30] C. Mourad, S. Elena, S. Abdelouahid, J. Marco-Contelles, J. Heterocycl. Chem. 47 (2010) 861–872.
[31] A.E. Mohamed, F.R. Hala, M.B. Doha, Y.E. Ibrahim, Eur. J. Med. Chem. 66 (2013) 415–422.
[32] F.M. Altalbawy, Int. J. Mol. Sci. 14 (2013) 2967–2979.
[33] S. Wenglowsky, K.A. Ahrendt, A.J. Buckmelter, B. Feng, S.L. Gloor, S. Gradl, J. Grina, J.D. Hansen, E.R. Laird, P. Lunghofer, S. Mathieu, Bioorg. Med. Chem. Lett. 21 (2011) 5533–5537.
[34] D. Bora, A. Kaushal, N. Shankaraiah, Eur. J. Med. Chem. 5 (2021) 113263.
[35] M. Benabdallah, O. Talhi, F. Nouali, N. Choukchou-Braham, K. Bachari, A. Silva, Curr. Med. Chem. 25 (2018) 3748–3767.
[36] L. Zhang, W. Ren, X. Wang, J. Zhang, J. Liu, L. Zhao, X. Zhang, Eur. J. Med. Chem. 126 (2017) 1071–1082.
[37] J. Khazir, P.P. Singh, D.M. Reddy, I. Hyder, S. Shafi, S.D. Sawant, G. Chashoo, A. Mahajan, M.S. Alam, A.K. Saxena, Eur. J. Med. Chem. 63 (2013) 279–289.
[38] C.R. Coxon, E. Anscombe, S.J. Harnor, M.P. Martin, B. Carbain, B.T. Golding, I. R. Hardcastle, L. K.Harlow, S. Korolchuk, C.J. Matheson, D.R. Newell, M.E. M. Noble, M. Sivaprakasam, S.J. Tudhope, D.M. Turner, L.Z. Wang, S.R. Wedge, C. Wong, R.J. Griffin, J.A. Endicott, C. Cano, J. Med. Chem. 60 (2017) 1746–1767.
[39] L. Duan, G. Feng, X. Wang, L. Wang, Q. Zhang, Phys. Chem. Chem. Phys. 19 (2017) 10140–10152.
[40] S. Bondock, N. Alabbad, A. Hossan, I.A. Shaaban, A.A. Shati, M.Y. Alfaifi, S. I. Elbehairi, R.H. Abd El-Aleam, M.M. Abdou, Chem. Biol. Interact. 407 (2025) 111366.
[41] D.A. Patel, S.S. Patel, H.D. Patel, *Bioorg. Chem.* 143 (2024) 107045.
[42] A.A. Mandour, I.F. Nassar, M.T. Abdel Aal, M.A. Shahin, W.A. El-Sayed, M. Hegazy, A.M. Yehia, A. Ismail, M. Hagras, E.B. Elkaeed, H.M. Refaat, J. Enzyme Inhib. Med. Chem. 37 (2022) 1957–1973.
[43] M.S. Elkotamy, M.K. Elgohary, A. Maher, M.A. Alkabbani, A.A. Almehizia, A. M. Naglah, H.A. Ghabbour, W.M. Eldehna, H.A. Abdel-Aziz, Bioorg. Chem. 7 (2025) 108565.
[44] I.F. Nassar, M.T. Aal, W.A. El-Sayed, M.A. Shahin, E.G. Elsakka, M.M. Mokhtar, M. Hegazy, M. Hagras, A.A. Mandour, N.S. Ismail, RSC Adv. 12 (2022) 14865–14882.
[45] S.M. Abou-seri, W.M. Eldehna, M.M. Ali, D.A. Abou, E. Ella, Eur. J. Med. Chem. 107 (2016) 165–179.
[46] S. Baumli, G. Lolli, E.D. Lowe, S. Troiani, L.A.N. Rusconi, EMBO. J. 27 (2008) 1907–1918.
[47] S.H. Lu, P.L. Liu, F.F. Wong, RSC Adv. 5 (2015) 47098–47107.

[48] J. Liu, H. Huang, X. Deng, R. Xiong, X. Cao, G. Tang, X. Wu, S. Xu, J. Peng, RSC Adv. 9 (2019) 2092–2101.
[49] https://doi.org/10.2210/pdb2A4L/pdb.
[50] W.F. De Azevedo, S. Leclerc, L. Meijer, L. Havlicek, M. Strnad, S.H. Kim, Eur. J. Biochem. 243 (1997) 518–526.
[51] G.M Ali, M.A. Ewida, A.M. Elmetwali, H.A Ewida, .R.F. George, W.R. Mahmoud, N. S. Ismail, M.S. Ahmed and, H.H. Georgey, RSC adv. 14 (2024) 34537–34555.
[52] P. Banerjee, E. Kemmler, M. Dunkel, R. Preissner, Nucleic Acids Res 52 (W1) (2024) W513–W520.
[53] H.A. Alomar, W.M. El Kady, A.A. Mandour, A.A. Naim, N.I. Ghali, T.A. Ibrahim, N. Fathallah, Results Chem. 14 (2025) 102081.
[54] M. Hagras, A.A. Abuelkhir, N.S. Abutaleb, A.M. Helal, I.M. Fawzy, M. Hegazy, M. N. Seleem, A.S. Mayhoub, RSC Adv. 14 (2024) 1513–1526.
[55] M. Moussaoui, M. Baassi, S. Baammi, H. Soufi, M. Salah, R. Daoud, A. El Allali, M. E. Belghiti, S. Belaaouad, J. Biomol. Struct. Dyn. 41 (2023) 13646–13662.